

# SIEMENS

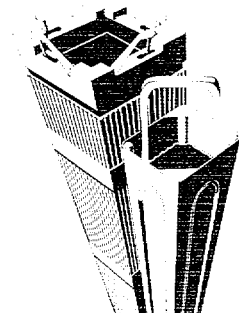
EMF-2403(NP)  
Revision 0

## Duplex D4 (DXD4) Cladding for PWRs

October 2000

Siemens Power Corporation  
Nuclear Division

---

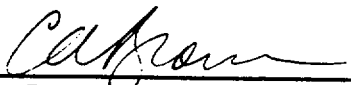
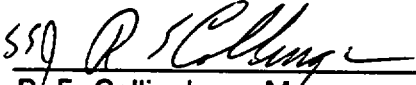
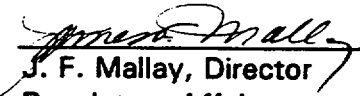


Siemens Power Corporation

ISSUED IN SPC ON-LINE  
DOCUMENT SYSTEM  
DATE: 10/26/00

EMF-2403(NP)  
Revision 0

Duplex D4 (DXD4) Cladding for PWRs

Prepared:	<u></u> L. F. Van Swam, Staff Engineer Engineering and Manufacturing	<u>9/25/2000</u> Date
Prepared:	<u></u> C. A. Brown, Team Leader Product Mechanical Engineering	<u>10-5-2000</u> Date
Reviewed:	<u></u> R. S. Reynolds, Director Research and Technology	<u>10/10/2000</u> Date
Approved:	<u></u> R. C. Gottula, Manager PWR Safety Analysis	<u>10/2/00</u> Date
Approved:	<u></u> R. E. Collingham, Manager Safety Analysis Methods	<u>10/3/00</u> Date
Approved:	<u></u> T. M. Howe, Manager Product Mechanical Engineering	<u>10-12-00</u> Date
Approved:	<u></u> J. F. Mallay, Director Regulatory Affairs	<u>10/10/00</u> Date

**U.S. Nuclear Regulatory Commission  
Report Disclaimer**

**Important Notice Regarding the Contents and Use of This Document**

***Please Read Carefully***

This technical report was derived through research and development programs sponsored by Siemens Power Corporation. It is being submitted by Siemens Power Corporation to the U.S. Nuclear Regulatory Commission as part of a technical contribution to facilitate safety analyses by licensees of the U.S. Nuclear Regulatory Commission which utilize Siemens Power Corporation fabricated reload fuel or technical services provided by Siemens Power Corporation for light water power reactors and it is true and correct to the best of Siemens Power Corporation's knowledge, information, and belief. The information contained herein may be used by the U.S. Nuclear Regulatory Commission in its review of this report and, under the terms of the respective agreements, by licensees or applicants before the U.S. Nuclear Regulatory Commission which are customers of Siemens Power Corporation in their demonstration of compliance with the U.S. Nuclear Regulatory Commission's regulations.

Siemens Power Corporation's warranties and representations concerning the subject matter of this document are those set forth in the agreement between Siemens Power Corporation and the Customer pursuant to which this document is issued. Accordingly, except as otherwise expressly provided in such agreement, neither Siemens Power Corporation nor any person acting on its behalf:

- a. makes any warranty or representation, express or implied, with respect to the accuracy, completeness, or usefulness of the information contained in this document, or that the use of any information, apparatus, method, or process disclosed in this document will not infringe privately owned rights;
- or
- b. assumes any liabilities with respect to the use of, or for damages resulting from the use of, any information, apparatus, method, or process disclosed in this document.

Duplex D4 (DXD4) Cladding for PWRs**Nature of Changes**

<u>Item</u>	<u>Page(s)</u>	<u>Description and Justification</u>
1.	All	This is a new document.

(This page was intentionally left blank.)

### **Acknowledgements**

The authors would like to express their appreciation to V. I. Arimescu, M. R. Billaux, W. C. Dey, J. A. Ford, J. S. Holm, R. Manzel, H.-J. Sell, and S.-H. Shann, for their participation in this project and for their significant contributions to the production of this document.

(This page was intentionally left blank.)

### **Abstract**

This report describes the manufacture, physical characteristics, and operational performance of a fuel rod cladding called Duplex D4, designated DXD4. The purpose of this report is to provide justification for the use of DXD4 cladding in PWR fuel reloads.

DXD4 cladding is a two-layer cladding consisting of a thin, highly corrosion-resistant outer layer of a low-tin, high-iron zirconium alloy, Alloy D4, bonded to a thicker inner layer of Zircaloy-4 that forms the bulk of the cladding and imparts most of its mechanical strength. The use of DXD4 cladding in PWRs provides for reductions in cladding corrosion, hydrogen pick-up, and fuel rod growth, and results in larger operating margins up to the approved fuel rod burnup limit of 62 MWd/kgU rod-average burnup.

This document is proprietary to Siemens and Siemens Power Corporation (SPC), and has been prepared to support a request by SPC for an exemption to 10 CFR 50.46 to permit the use of DXD4 as a fuel rod cladding in addition to other approved zirconium alloy claddings. Data and analytical models not previously disclosed in the public domain remain the property of SPC and Siemens.

(This page was intentionally left blank.)

## Contents

1.0	Introduction .....	1
2.0	Summary .....	3
3.0	Design Description .....	5
4.0	Evaluation of Cladding .....	9
4.1	Fuel System Damage .....	9
4.1.1	Design Stress .....	9
4.1.2	Design Strain .....	11
4.1.3	Strain Fatigue .....	14
4.1.4	Fretting Wear .....	15
4.1.5	Oxidation, Hydrogen Pick-up, and Crud Buildup .....	15
4.1.6	Rod Bowing .....	20
4.1.7	Axial Growth .....	21
4.1.8	Rod Internal Pressure .....	24
4.1.9	Assembly Liftoff .....	25
4.1.10	Control Rod Reactivity .....	26
4.2	Fuel Rod Failure .....	26
4.2.1	Hydriding (Internal) .....	26
4.2.2	Cladding Collapse .....	27
4.2.3	Overheating of Cladding .....	29
4.2.4	Overheating of Fuel Pellets .....	30
4.2.5	Pellet-Cladding Interaction .....	31
4.2.6	Cladding Rupture and Ballooning .....	32
4.2.7	Fuel Rod Mechanical Fracturing .....	34
4.2.8	Excessive Enthalpy .....	34
4.3	Fuel Coolability .....	35
4.3.1	Fragmentation of Embrittled Cladding .....	35
4.3.2	Violent Expulsion of Fuel .....	40
4.3.3	Cladding Ballooning .....	41
4.3.4	Fuel Assembly Structural Damage from External Forces .....	41
5.0	Design Analysis .....	43
5.1	Introduction .....	43
5.2	Description of Fuel Design Analyses .....	43
5.2.1	Cladding Collapse .....	43
5.2.2	Overheating of Fuel Pellets .....	44
5.2.3	Pellet-Cladding Interaction .....	44
5.2.4	Cladding Stresses .....	45
5.2.5	Cladding Strain .....	45
5.2.6	Fatigue .....	46
5.2.7	Oxidation, Hydriding, and Crud Buildup .....	46

Duplex D4 (DXD4) Cladding for PWRs

5.2.8	Fuel Rod Growth .....	46
5.2.9	Rod Internal Pressure .....	47
5.3	Results of Fuel Design Analysis .....	47
5.4	Conclusions .....	48
6.0	Operational Experience .....	53
7.0	Material Properties .....	61
7.1	Basic Properties Of Cladding .....	61
7.1.1	As-Manufactured Cladding Properties .....	61
7.1.2	Iodine Stress Corrosion Cracking Behavior .....	61
7.2	Correlations and Model Parameters Used for Fuel Performance Analysis .....	61
7.2.1	Density .....	61
7.2.2	Thermal Expansion .....	62
7.2.3	Thermal Conductivity .....	62
7.2.4	Young's Modulus and Poisson's Ratio .....	63
7.2.5	Thermal and Irradiation-Induced Creep .....	63
7.2.6	Irradiation-Induced Growth .....	64
7.2.7	Fatigue Design Curve .....	64
7.3	LOCA-Related Properties: Specific Heat and Enthalpy .....	64
8.0	References .....	71
Appendix A	Thermal Creep of DXD4 Cladding .....	A-1
Appendix B	Corrosion Behavior of DXD4 Cladding .....	B-1
B.1.	Oxidation .....	B-1
B.2.	Corrosion Model .....	B-3
B.3.	Corrosion Model Verification .....	B-6
B.4.	Conclusions .....	B-8
B.5.	References .....	B-8
Appendix C	Hydrogen Pick-up and Hydride Distribution .....	C-1
C.1.	Introduction .....	C-1
C.2.	Experimental Results .....	C-2
C.3.	Discussion .....	C-3
C.4.	Metallographic Observations .....	C-4
C.5.	Conclusions .....	C-6
C.6.	References .....	C-6

<b>Appendix D</b>	<b>Stress Rupture and Ballooning Tests .....</b>	<b>D-1</b>
D.1.	Introduction .....	D-1
D.2.	Test Description .....	D-2
D.3.	Specimen Design .....	D-2
D.4.	Testing Procedure .....	D-3
D.5.	Comparative Stress Rupture Behavior.....	D-4
D.6.	Comparative Ballooning Behavior.....	D-5
<b>Appendix E</b>	<b>High-Temperature Corrosion and Quench Behavior .....</b>	<b>E-1</b>
E.1.	Introduction .....	E-1
E.2.	Experimental Design .....	E-2
E.3.	Test Program .....	E-3
E.4.	Test Results .....	E-4
E.5.	Conclusions .....	E-6
E.6.	References.....	E-7

(This page was intentionally left blank.)

## Tables

<b>Table 3.1</b>	<b>Chemical Composition of Duplex D4 Cladding.....</b>	<b>6</b>
<b>Table 4.1.1.1</b>	<b>Comparison of Circumferential and Axial Bending Strength .....</b>	<b>11</b>
<b>Table 5.1</b>	<b>Fuel Rod Design Analysis Calculation Results .....</b>	<b>49</b>
<b>Table 6.1</b>	<b>Operating Experience of Siemens PWR Fuel with Duplex Cladding (April 2000).....</b>	<b>55</b>
<b>Table 6.2</b>	<b>Operating Experience of Siemens PWR Fuel with Duplex B (ELSO.8B) Cladding (April 2000) .....</b>	<b>56</b>
<b>Table 6.3</b>	<b>Operating Experience of Siemens PWR Fuel with Duplex D4 Cladding (April 2000).....</b>	<b>57</b>
<b>Table 6.4</b>	<b>Fuel Rod Parameters and Core Operating Conditions for PWRs with DXD4 Fuel Assemblies .....</b>	<b>57</b>
<b>Table 7.1</b>	<b>Characteristics of Manufactured DXD4 Cladding Lots .....</b>	<b>65</b>
<b>Table 7.2</b>	<b>Measured and Calculated Creepdown Permanent Strains for DXD4 Clad Fuel Rods .....</b>	<b>69</b>
<b>Table A.1</b>	<b>Creep Strain (%) During Biaxial Creep Tests at 382°C and 120 MPa Circumferential Stress for DXD4 and Zircaloy-4 Claddings .....</b>	<b>A-3</b>
<b>Table B.1</b>	<b>Operating Conditions of PWRs Where DXD4 Cladding Corrosion Was Measured .....</b>	<b>B-9</b>
<b>Table B.2</b>	<b>DXD4 Fuel Rod Maximum Oxide Thickness, Line-Contact Method .....</b>	<b>B-10</b>
<b>Table B.3</b>	<b>DXD4 Fuel Rod Maximum Oxide Thickness, Point-Contact Method .....</b>	<b>B-11</b>
<b>Table B.4</b>	<b>Maximum Oxide Thickness of DXD4 Fuel Rods Irradiated at Plant B42 .....</b>	<b>B-14</b>
<b>Table C.1</b>	<b>Hydrogen Pick-up Data for DXD4 Cladding at PWR D18 .....</b>	<b>C-2</b>
<b>Table D.1</b>	<b>Zircaloy-4 Cladding Source and Properties .....</b>	<b>D-6</b>
<b>Table D.2</b>	<b>Stress Rupture and Clad Swelling Test Results for Zircaloy-4 Cladding with a Nominal Tin Content of 1.3% .....</b>	<b>D-7</b>
<b>Table D.3</b>	<b>Stress Rupture and Clad Swelling Test Results for Duplex D4 (DXD4) Cladding.....</b>	<b>D-10</b>
<b>Table D.4</b>	<b>Stress Rupture and Clad Swelling Test Results for Duplex B (DXB) Cladding.....</b>	<b>D-11</b>
<b>Table E.1</b>	<b>Cladding Source and Chemical Composition Records for High- Temperature Corrosion and Quench Test Specimens.....</b>	<b>E-8</b>
<b>Table E.2</b>	<b>Results of High-Temperature Corrosion Tests on Through-Wall Zircaloy-4 Cladding.....</b>	<b>E-9</b>
<b>Table E.3</b>	<b>Results of High-Temperature Corrosion Tests on Duplex D4 Cladding .....</b>	<b>E-10</b>

(This page was intentionally left blank.)

## Figures

<b>Figure 3.1</b>	Duplex Cladding Fabrication Process Outline.....	7
<b>Figure 4.1.2.1</b>	RODEX2 Creepdown Benchmarking Results for DXD4 Cladding .....	13
<b>Figure 4.1.5.1</b>	DXD4 Cladding Oxide Thickness as a Function of Burnup .....	17
<b>Figure 4.1.5.2</b>	Comparison of Measured and CORROS II-Calculated Oxide for Five PWR Plants.....	18
<b>Figure 4.1.5.3</b>	Oxide Thickness as a Function of Burnup for Plant D24 .....	19
<b>Figure 4.1.5.4</b>	Hydrogen Pick-up as a Function of Oxide Thickness.....	20
<b>Figure 4.1.7.1</b>	Optimized Zircaloy-4 Fuel Rod Growth as a Function of Fast Fluence.....	22
<b>Figure 4.1.7.2</b>	Duplex D4 Fuel Rod Growth as a Function of Fast Fluence.....	23
<b>Figure 4.1.7.3</b>	Comparison of Optimized Zircaloy-4 and Duplex D4 Fuel Rod Growth as a Function of Fast Fluence.....	23
<b>Figure 4.2.2.1</b>	Helical Diameter Scan of a One-Cycle DXD4 Fuel Rod .....	29
<b>Figure 4.2.6.1</b>	Time to Rupture of DXD4 and DXB Cladding as a Function of Temperature and Initial Cladding Hoop Stress .....	33
<b>Figure 4.2.6.2</b>	Rupture Hoop Strain of DXD4 and DXB Cladding Compared to the Standard Zircaloy-4 Cladding Reference Maximum Hoop Strain.....	33
<b>Figure 4.3.1.1</b>	Comparison of Weight Gain as a Function of Time for Through-Wall Zircaloy-4 and Duplex D4 Cladding.....	36
<b>Figure 4.3.1.2</b>	Duplex D4 Cladding Exposed for One (1) Minute at 1050°C.....	37
<b>Figure 4.3.1.3</b>	Through-Wall Zircaloy-4 Cladding Exposed for Ten (10) Minutes at 1050°C.....	38
<b>Figure 4.3.1.4</b>	Duplex D4 Cladding Exposed for Ten (10) Minutes at 1250°C.....	39
<b>Figure 5.1</b>	Power Histories of the Most-Limiting DXD4 Rods for Corrosion and Rod Internal Pressure Calculations .....	50
<b>Figure 5.2</b>	Power Histories of the Most-Limiting DXD4 Rods for Collapse, AOO Strain, and Steady-State Strain Calculations .....	50
<b>Figure 5.3</b>	Corrosion Predictions for the Most-Limiting Urania and Urania/Gadolinia DXD4 Fuel Rods.....	51
<b>Figure 5.4</b>	Rod Internal Pressure Predictions for the Most-Limiting Urania and Urania/Gadolinia DXD4 Fuel Rods.....	51
<b>Figure 6.1</b>	Burnup Distribution of Siemens PWR Fuel with Duplex Cladding (April 2000).....	58
<b>Figure 6.2</b>	Burnup Distribution of Siemens PWR Fuel with Duplex B (ELS0.8B) Cladding (April 2000) .....	58

## Duplex D4 (DXD4) Cladding for PWRs

<b>Figure 6.3</b> Burnup Distribution of Siemens PWR Fuel with Duplex D4 Cladding (April 2000).....	59
<b>Figure B.1</b> DXD4 Cladding Oxide Thickness as a Function of Burnup.....	B-15
<b>Figure B.2</b> Measured Axial Oxide Profile for Plant D24, Assembly 16-01, Rod L05 through Successive Cycles of Irradiation .....	B-15
<b>Figure B.3</b> Measured Axial Oxide Profile for Plant D24, Assembly 16-01, Rod L02 through Successive Cycles of Irradiation .....	B-16
<b>Figure B.4</b> Measured Axial Oxide Profile for Plant D24, Assembly 16-01, Rod L01 through Successive Cycles of Irradiation .....	B-16
<b>Figure B.5</b> Measured Axial Oxide Profile for Plant D18, Assembly 0366, Rod N14 after Four Cycles of Irradiation.....	B-17
<b>Figure B.6</b> Measured Axial Oxide Profile for Plant D18, Assembly 0366, Rod R13 after Four Cycles of Irradiation.....	B-17
<b>Figure B.7</b> Typical Fuel Rod Power Histories for Plants D18 and D24 .....	B-18
<b>Figure B.8</b> DXD4 Cladding Oxide Predictions for Plant D24 without the Second- Transition Model Compared to Measured Data, Indicating Underprediction at High Burnup.....	B-18
<b>Figure B.9</b> Comparison of Measured and CORROS II-Calculated Oxide for Plants D18, D21, and D24 .....	B-19
<b>Figure B.10</b> Comparison of Measured Oxide Thickness and Predicted Best-Estimate and 95/95 Upper-Bound Corrosion of Plant D18 Fuel Rods.....	B-20
<b>Figure B.11</b> Comparison of Measured Oxide Thickness and Predicted Best-Estimate and 95/95 Upper-Bound Corrosion of Plant D24 Fuel Rods.....	B-20
<b>Figure B.12</b> Comparison of Measured and CORROS II-Calculated Oxide for Plants B42 and D14 .....	B-21
<b>Figure B.13</b> Measured Axial Oxide Profile and CORROS II-Calculated Data for Plant D24, Assembly 16-01, Rod L05 through Successive Cycles of Irradiation .....	B-22
<b>Figure B.14</b> Measured Axial Oxide Profile and CORROS II-Calculated Data for Plant D24, Assembly 16-01, Rod L02 through Successive Cycles of Irradiation .....	B-22
<b>Figure B.15</b> Measured Axial Oxide Profile and CORROS II-Calculated Data for Plant D24, Assembly 16-01, Rod L01 through Successive Cycles of Irradiation .....	B-23
<b>Figure B.16</b> Measured Axial Oxide Profile and CORROS II-Calculated Data for Plant D18, Assembly 0366, Rod N14 after Four Cycles of Irradiation .....	B-23
<b>Figure B.17</b> Measured Axial Oxide Profile and CORROS II-Calculated Data for Plant D18, Assembly 0366, Rod R13 after Four Cycles of Irradiation .....	B-24
<b>Figure C.1</b> Hydrogen Pick-up Fraction as a Function of Oxide Thickness .....	C-7
<b>Figure C.2</b> Hydrogen Pick-up as a Function of Oxide Thickness .....	C-7
<b>Figure C.3</b> Hydride Distribution and Oxide Layer in DXD4 Clad Fuel Rod A09 .....	C-8

<b>Figure C.4</b>	Hydride Distribution and Oxide Layer in DXD4 Clad Fuel Rod G01 .....	C-8
<b>Figure C.5</b>	Hydride Distribution and Oxide Layer in DXD4 Clad Fuel Rod R12 .....	C-9
<b>Figure C.6</b>	Hydride Distribution and Oxide Layer in Zircaloy-4 Clad Fuel Rod V04 .....	C-9
<b>Figure C.7</b>	Hydride Distribution and Oxide Layer in Zircaloy-4 Clad Fuel Rod V04 .....	C-10
<b>Figure D.1</b>	Schematic Representation of Stress Rupture and Ballooning Test Experimental Setup .....	D-12
<b>Figure D.2</b>	Stress Rupture and Ballooning Specimen Design (left) and Thermocouple Locations (center and right).....	D-13
<b>Figure D.3</b>	Change of Temperature and Pressure as a Function of Time in the Stress Rupture Test .....	D-14
<b>Figure D.4</b>	Typical Evolution of Strain During a Stress Rupture Test .....	D-14
<b>Figure D.5</b>	Time to Rupture of Low-Tin Zircaloy-4 Cladding as a Function of Temperature and Initial Specimen Pressure .....	D-15
<b>Figure D.6</b>	Time to Rupture of Standard-Tin (1.5% Sn) and Low-Tin (1.3% Sn) Zircaloy-4 Cladding as a Function of Temperature and Initial Cladding Hoop Stress <i>(These data are used to establish the least-squares fit reference lines for Zircaloy-4 cladding)</i> .....	D-15
<b>Figure D.7</b>	Time to Rupture of DXD4 and DXB Cladding as a Function of Temperature and Initial Cladding Hoop Stress. <i>(The lines represent the Zircaloy-4 cladding reference correlations established earlier.)</i> .....	D-16
<b>Figure D.8</b>	Hoop Strain at Rupture of Zircaloy-4 Cladding with a Nominal Tin Content of 1.5%. <i>(The upper-bound curve is the Zircaloy-4 cladding reference maximum hoop strain.)</i> .....	D-16
<b>Figure D.9</b>	Hoop Strain at Rupture of Low-Tin Zircaloy-4 Cladding Compared to the Standard Zircaloy-4 Cladding Reference Maximum Hoop Strain.....	D-17
<b>Figure D.10</b>	Rupture Hoop Strain of DXD4 and DXB Cladding Compared to the Standard Zircaloy-4 Cladding Reference Maximum Hoop Strain.....	D-17
<b>Figure E.1</b>	Apparatus for the Determination of High-Temperature Steam Oxidation Kinetics of Zirconium Alloy Cladding.....	E-11
<b>Figure E.2</b>	Typical Example of Cladding Specimen Temperature as a Function of Time During a High-Temperature Oxidation and Quench Test .....	E-11
<b>Figure E.3</b>	Weight Gain as a Function of Time for Through-Wall Zircaloy-4 Cladding ...	E-12
<b>Figure E.4</b>	Weight Gain as a Function of Time for Duplex D4 Cladding.....	E-12
<b>Figure E.5</b>	Comparison of Weight Gain as a Function of Time for Through-Wall Zircaloy-4 and Duplex D4 Cladding.....	E-13
<b>Figure E.6</b>	Thickness of the Oxide Scale on the Zircaloy-4 Inner Surface and D4- Alloy Outer Surface of Duplex D4 Cladding Specimens. <i>(The thickness of the oxide scale on both surfaces is identical.)</i> .....	E-13

<b>Figure E.7</b> Thickness of the Oxygen-Stabilized $\alpha$ -Layer of the Zircaloy-4 Inner Surface and D4-Alloy Outer Surface of Duplex D4 Cladding Specimens. <i>(Oxygen penetration is, in general, somewhat greater in Zircaloy-4 than in the D4 Alloy.)</i> .....	E-14
<b>Figure E.8</b> Duplex D4 Cladding Exposed for Ten (10) Minutes at 1050°C.....	E-15
<b>Figure E.9</b> Duplex D4 Cladding Exposed for Five (5) Minutes at 1050°C .....	E-16
<b>Figure E.10</b> Duplex D4 Cladding Exposed for Two (2) Minutes at 1050°C.....	E-17
<b>Figure E.11</b> Duplex D4 Cladding Exposed for One (1) Minute at 1050°C.....	E-18
<b>Figure E.12</b> Duplex D4 Cladding Exposed for Ten (10) Minutes at 1150°C.....	E-19
<b>Figure E.13</b> Duplex D4 Cladding Exposed for Two (2) Minutes at 1150°C.....	E-20
<b>Figure E.14</b> Duplex D4 Cladding Exposed for One (1) Minute at 1150°C.....	E-21
<b>Figure E.15</b> Duplex D4 Cladding Exposed for Ten (10) Minutes at 1250°C.....	E-22
<b>Figure E.16</b> Duplex D4 Cladding Exposed for Two (2) Minutes at 1250°C.....	E-23
<b>Figure E.17</b> Duplex D4 Cladding Exposed for One (1) Minute at 1250°C.....	E-24

**Nomenclature**

<u>Acronym / Term</u>	<u>Definition</u>
ADU	Ammonium diuranate
ASME	American Society of Mechanical Engineers
ASTM	American Society for Testing and Materials
BOC	Beginning-of-cycle
BWR	Boiling water reactor
CEA	Control element assembly
CFR	Code of Federal Regulations
D4	Corrosion-resistant zirconium alloy
DNB	Departure from nucleate boiling
DNBR	Departure from nucleate boiling ratio
Duplex	Cladding consisting of two layers metallurgically bonded together
DXB	Duplex B cladding
DXD4	Duplex D4 cladding: Duplex cladding with a Zircaloy-4 inner layer and a D4 outer layer
ECR	Equivalent clad reacted
LHGR	Linear heat generation rate
LOCA	Loss-of-coolant accident
LTA	Lead test assembly
MOX	Mixed oxide
MWd/kgU	Megawatt-days per kilogram of uranium
PCI	Pellet-cladding interaction
PWR	Pressurized water reactor
SPC	Siemens Power Corporation
SRP	Standard Review Plan

Duplex D4 (DXD4) Cladding for PWRs

---

(This page was intentionally left blank.)

## 1.0 Introduction

One of the limiting factors in the burnup of pressurized water reactor fuel is corrosion of the fuel rod cladding due to exposure to the reactor coolant. Siemens has developed a two-layer fuel rod cladding that provides improved resistance to such corrosion. This cladding has been specifically designed to successfully endure the high temperatures and long exposure times associated with high fuel burnup.

The material used for this cladding, called Duplex D4 (or DXD4), consists of a thin, highly corrosion-resistant outer layer that is bonded by co-extrusion to a much thicker inner layer of Zircaloy-4. The outer layer is a zirconium alloy with an extra-low-tin, high-iron, high-chromium chemical composition compared to Zircaloy-4. While the outer layer provides exceptional corrosion resistance, the inner layer ensures that the cladding maintains the necessary mechanical and creep strength.

Siemens Power Corporation (SPC) has prepared this report to describe the manufacture, physical characteristics, and operational performance of DXD4 cladding. The report provides the technical bases for using DXD4 cladding in PWR reload fuel, and describes the corrosion and cladding growth equations developed specifically for this cladding.

SPC requests the NRC's approval to use DXD4 cladding in PWRs up to a rod-average burnup of 62 MWd/kgU, and also requests approval to apply the corrosion and cladding growth equations presented in this report for the DXD4 cladding.

(This page was intentionally left blank.)

## 2.0 Summary

This report describes Duplex D4 (DXD4) cladding, its manufacture and physical characteristics, and its performance relative to established design criteria. SPC developed a topical report (Reference 1) that was approved by the NRC, which establishes a set of design criteria for PWR fuel that is consistent with Chapter 4 of the Standard Review Plan (SRP) (Reference 2). In cases where the SPC criteria are either more specific or more conservative than the SRP criteria, the SPC criteria are used for the evaluation. An example fuel rod analysis in which DXD4 cladding is used has been evaluated against SPC's criteria; the results are provided in Section 5. Extensive operational experience and problem-free performance of approximately 580,000 Duplex rods (including 21,000 DXD4 rods) in 15 PWRs, up to peak assembly burnups of 62 MWd/kgU [

], are also described. (Although problem-free operational experience of DXD4 cladding extends to [ ], these highest-burnup data were not available when the analyses presented in this report were performed.) These evaluations and experience demonstrate that DXD4 is an acceptable fuel rod cladding, suitable for use under demanding conditions.

DXD4 is a medium-/high-tin Zircaloy-4 cladding, which meets ASTM specifications, with an outer corrosion-resistant layer of very-low-tin zircaloy. The inner layer, which accounts for most of the wall thickness, provides the bulk of the strength for the cladding and, except for performance related to exposure to reactor coolant, mainly defines its in-reactor properties and behavior. The outer layer of the cladding is specifically designed to resist corrosion, and is shown to experience a maximum oxidation, at a 95/95 confidence level, of about [ ] microns at 62 MWd/kgU rod burnup.

DXD4 cladding has been evaluated against the criteria in SPC's topical report on generic mechanical design criteria for PWRs. The evaluation demonstrates that DXD4 cladding can be conservatively evaluated using the same criteria and design analysis models used for cladding consisting only of Zircaloy-4. The performance of DXD4 is superior to that of Zircaloy-4 in the areas of fuel rod growth and fuel cladding external corrosion. The maximum axial growth of DXD4 cladding is about [ ] than expected for Zircaloy-4. External oxidation is greatly improved over Zircaloy-4, showing a reduction in maximum

corrosion relative to Zircaloy-4 of about [     ]. Revised design analysis models are presented and justified for fuel rod growth and fuel cladding external corrosion. In design analyses, SPC will treat DXD4 cladding as Zircaloy-4 cladding, except that the DXD4 growth and corrosion models presented herein will be used.

The performance of DXD4 cladding has been tested and evaluated with respect to its behavior during a LOCA. The key conclusions from that evaluation are: . . .

- The metal-water reaction correlations applicable to Zircaloy-4 during a LOCA are conservatively applicable to DXD4 cladding.
- The stress rupture behavior of DXD4 cladding during a LOCA is equivalent to that of through-wall Zircaloy-4.
- The embrittlement criteria specified by 10 CFR 50.46 are applicable to DXD4 cladding.

### 3.0 Design Description

In the mid- to late-1980s, Siemens developed the Duplex cladding concept. In this cladding, Zircaloy-4 forms an inner layer which constitutes the bulk of the wall thickness; the outer layer of the cladding wall consists of a different, highly corrosion-resistant zirconium-based alloy. The two layers are metallurgically bonded together, typically by high-temperature co-extrusion at an intermediate fabrication stage in the tubing manufacturing process.

Duplex cladding tubes are manufactured with the same diameters, wall thicknesses, and tolerances as standard through-wall cladding tubes such that the neutronic and thermal-hydraulic design of a given assembly will not be affected by switching from Zircaloy-4 to Duplex cladding.

Duplex cladding offers the advantage that the corrosion properties, which are determined by the outer layer of the cladding, can be de-coupled from the mechanical properties, which are determined by the much thicker inner layer of Zircaloy-4. This provides a cladding in which the corrosion performance and the mechanical performance can be optimized independent of one another.

An outline of the Duplex cladding fabrication process used by one of Siemens' vendors is shown in Figure 3.1. Both the outer-layer material and the inner-layer material (Zircaloy-4) are processed via the conventional routes of melting, forging, quenching, and annealing to the billet stage. The billet for the outer layer is then pierced and extruded to form a large-diameter tube, or shell. After machining, the billet for the inner layer and the outer layer shell are joined and co-extruded to form a thick-wall tube approximately three inches in diameter. After the co-extrusion process, the tubing is examined by ultrasound to assure that no flaws or bonding defects are present between the two layers. Subsequent pilgering (cold rolling) of the large-diameter tube in several steps with intermediate anneals to the final cladding size follows the normal fabrication schedule of the tubing manufacturer.

Siemens has tested Duplex claddings with different composition zirconium alloy outer layers. The alloy for the outer layer designated D4 nominally consists of zirconium with

[ ]]. The Duplex cladding with a Zircaloy-4 inner and a D4 outer layer is designated Duplex D4, or DXD4. The chemical compositions of the inner and outer layers of DXD4 are given in Table 3.1. For comparison, the typical composition ranges of the alloying elements in Optimized (Siemens low-tin) Zircaloy-4 and the ranges specified by ASTM for Zircaloy-4 are also provided.

[

]

**Table 3.1 Chemical Composition of Duplex D4 Cladding**

Alloying Element	Chemical Composition (%)			
	DXD4 Outer Layer: D4 Alloy	DXD4 Inner Layer: Zircaloy-4	Optimized Zircaloy-4	ASTM Specification
Tin (Sn)	[ ]	[ ]	[ ]	1.20 – 1.70
Iron (Fe)	[ ]	[ ]	[ ]	0.18 – 0.24
Chromium(Cr)	[ ]	[ ]	[ ]	0.07 – 0.13
Nickel (Ni)	[ ]	---	---	---
Oxygen (O)	[ ]	[ ]	[ ]	Not specified
Silicon (Si)	[ ]	[ ]	[ ]	<0.0120

Duplex D4 (DXD4) Cladding for PWRs

---



**Figure 3.1 Duplex Cladding Fabrication Process Outline**

(This page was intentionally left blank.)

## 4.0 Evaluation of Cladding

### 4.1 *Fuel System Damage*

#### 4.1.1 Design Stress

The design basis for fuel cladding stresses specifies that the fuel system will not be damaged due to excessive stresses. Conservative limits are derived from the ASME Boiler Code (Code), Section III, Division 1, Article III-2000 (see Reference 3). The stress limits are based on the minimum specified 0.2% offset yield strength and the ultimate strength of the unirradiated cladding (Reference 1, Section 3.2.5).

The specified strength is evaluated with axial tensile tests; per the Code, combined stresses in the cladding are evaluated with the maximum shear stress criterion (Tresca criterion). The material properties of DXD4 cladding are specified on the same basis as through-wall Zircaloy-4 cladding, and [

].

Although the corrosion-resistant outer layer of Duplex D4 cladding has less mechanical strength than the Zircaloy-4 inner layer, the [

]. Thus, in a uniform tensile test, the combined properties of the inner and outer layers of DXD4 cladding are approximately equivalent to those of Optimized Zircaloy-4 and meet the same specification limits. DXD4 cladding will be evaluated on the same basis (using the same specification properties) as through-wall Zircaloy-4 cladding.

The properties of DXD4 cladding in bending, particularly in circumferential bending, however, may differ from those of Zircaloy-4 cladding due to the disposition of the D4 alloy on the outer fiber of the clad. In this disposition, a higher proportion of the bending stresses (e.g., from ovality pressure bending stresses and spacer contact bending stresses) are imposed toward the clad inner and outer surfaces (highest fiber stresses). This disposition of bending stresses preferentially loads the Duplex layer. To evaluate this behavior, ovality bending tests and comparative tensile tests were performed for DXD4 cladding and two through-wall Zircaloy-4 claddings with comparable dimensions. The

tests consisted of laterally compressing clad segments (0.424 inch diameter, 3 inches long) between flat platens at room temperature and at elevated temperature.

Force-deflection curves were evaluated for each of the materials at each test temperature. The relative bending strength of the DXD4 material was slightly reduced compared to the through-wall materials; however, all the clad types showed substantially greater strength in the circumferential direction than predicted from the axial tensile tests.

The cladding's greater strength in the circumferential direction is due to the anisotropy of the material and to conservatism in the use of the maximum shear stress criterion for stress evaluation, rather than the Von Mises criterion (distortion energy criterion). The material is inherently stronger in the circumferential direction (as also demonstrated by the high circumferential ultimate stress determined in the burst test), and when clad lengths are loaded in circumferential bending, the Von Mises criterion can show higher yield, up to 15%, for the combined-stress state that occurs. This combined-stress state is also typical for the stress state during fuel clad operation. Both of these factors contribute to the measured minimum [ ] greater strength of DXD4 in the circumferential direction and the approximately [ ] greater strength of the through-wall materials.

Table 4.1.1.1 shows the ratio of the ovality bending stress at the first departure from linearity (see Reference 4 for calculation of two-point ring bending stress) to the measured axial 0.2% yield stress. The first departure from linearity of the load-deflection plot is taken as the yield point for the ovality bending test. Normalization for small variations in sample geometry, tube thickness, and diameter are taken into consideration by calculating the bending stress for the test load. Determining the ratio of ovality bending yield stress to axial tensile yield stress for each material allows normalization for variations in heat treatment and thus final material strength. A ratio of the bending stress in the plastic regime to the ultimate axial tensile stress is also determined.

The ratio of circumferential to axial strengths thus determined is greater than unity, indicating that the tubing has greater circumferential strength than axial strength. This benefit is smallest for the DXD4 cladding; on average, the ratio was [ ] less than that for through-wall Zircaloy-4 cladding at room temperature, and [ ] less at 382°C. However,

the circumferential bending strength of the DXD4 cladding remains [ ] greater at room temperature and [ ] greater at 382°C than the axial strength (which is specified in the DXD4 cladding specification).

These test results demonstrate the conservatism in the use of the current methodology based on tensile stress limits for evaluating circumferential bending stresses. For the design evaluation of DXD4 cladding, the existing practice of using the tensile properties for establishing the stress limit is conservative and will therefore be retained for evaluation of Duplex clad stresses where the outside (Duplex) layer thickness does not substantially [ ] of the overall cladding wall thickness.

**Table 4.1.1.1 Comparison of Circumferential and Axial Bending Strength**

#### 4.1.2 Design Strain

The SRP does not suggest specific limits for cladding strain. SPC's design criteria for fuel rod cladding strain (Reference 1) specify that the total mean circumferential strain shall not exceed 1% for local burnups less than 60 MWd/kgU and 0.75% for burnups greater than 60 MWd/kgU (Reference 1, Section 3.2.5).

The methodology used to prove that the cladding strain design criteria are met involves the use of the RODEX2 code (Reference 5) to simulate the most demanding power histories

with the most conservative combination of pellet and cladding properties in order to maximize end-of-life cladding strain. In order to justify RODEX2 applicability to the analysis of the design strain criteria, SPC performed the two evaluations presented below and in Appendix A.

First, in order to show that the increase in the effective creep rate – due to the higher creep strain rate of the outer (D4) material – is only marginal, the range of effective creep strain rates of the two-layered DXD4 cladding was evaluated based on a simplified theoretical model and measured mechanical properties of the materials composing the two layers. This analysis showed that the expected increase in creep rate would be in the range of [ ] (maximum values of [ ]). This increase is minimal, and well within the variability of the total strain of typical through-wall cladding.

Second, the measured circumferential strains for rods with DXD4 cladding at different burnups up to 60 MWd/kgU were compared with RODEX2 calculations to prove that RODEX2 evaluations are conservative with respect to the end-of-life design strain. The agreement of calculated strains with measured post-irradiation strains also showed that irradiation creep of DXD4 cladding is not adversely affected by the slightly different composition of the outer layer (see Section 7.2.5). This result is also expected because the average tin content of DXD4 cladding, which largely determines the creep properties of zircaloy-type alloys, is within the ASTM-specified range for zircaloy and meets the requirements of Optimized Zircaloy-4 cladding.

The results of the RODEX2 benchmarking are presented in Figure 4.1.2.1.

Two types of creepdown were reported (and correspondingly marked in the figure) in fuel examination reports: 1) average creepdown over the central fuel rod spans, and 2) maximum creepdown (minimum strain) of the middle sections of all central spans. The RODEX2 predictions agree well with the average creepdown values (circumferential strains) and are slightly less than the measured maximum creepdown values. This qualifies RODEX2 calculations as a conservative prediction of the end-of-life total strain.



#### Figure 4.1.2.1 RODEX2 Creepdown Benchmarking Results for DXD4 Cladding

The group of fuel rods measured for RODEX2 creepdown benchmarking includes rods with pellets fabricated using SPC's patented dry conversion process, as well as rods containing pellets derived from the ammonium diuranate (ADU) "wet" process. Both types of pellets are comparable in terms of initial density and densification characteristics. Rod diameters after irradiation depend on both cladding creepdown and pellet expansion after the initial densification is completed. Figure 4.1.2.1 shows that the strain reversal point (after pellet-cladding contact is firmly established) is accurately predicted for the rods in Plants D14 and D18. For the D18 rods, the combination of a smaller as-fabricated fuel rod diameter and the same diametrical pellet-cladding gap as the D14 rods leads to a small delay in the onset of strain reversal; this is adequately simulated by RODEX2. Plant D24 cladding strains were measured after one irradiation cycle, when the cladding had not yet come into full contact with the fuel pellets and was still creeping down. The RODEX2-calculated strain values are in close agreement with the measurements, proving that the combined contributions of thermal and irradiation creep strains in this case are also adequately described for the DXD4 cladding by the standard RODEX2 creep equation.

#### 4.1.3 Strain Fatigue

Cladding fatigue analysis is based on the cyclic stress amplitudes calculated for the specified number of duty cycles during the irradiation life, using the conservative O'Donnell and Langer (Reference 6) fatigue design curve. This curve includes a safety factor of 2 on stress amplitude or a safety factor of 20 on the number of cycles, whichever is more conservative.

The methodology to evaluate the stress cycles is based on the RODEX2 and RAMPEX codes. The RODEX2 code is used to calculate the pseudo-steady-state deformations of the pellet and cladding; the RAMPEX code uses the RODEX2-calculated deformations as the starting point for calculating stresses and strains during power ramps. Changes in clad stress are evaluated to determine a fatigue usage factor, which is conservatively limited to 0.67 (Reference 1, Section 3.3.2). As discussed in Section 4.1.2, the RODEX2 code is equally applicable to both Duplex and through-wall Zircaloy-4 claddings.

During power ramps, the strain in the cladding is not affected by possible slight cladding material variations because the total strain is imposed by the expanding pellet and, therefore, is not dependent on the properties of the clad.

The strain fatigue design criterion of O'Donnell and Langer is furthermore applicable, because it considers stresses evaluated at maximum mean clad strain and hence is not influenced by the lower yield strength of the Duplex layer. The D4 alloy used in the outer layer of DXD4 cladding has a composition very similar to [

].

Therefore, considering that DXD4 clad has the same overall deflection behavior as through-wall Zircaloy-4, the methods used to calculate fatigue stresses for Zircaloy-4 cladding are applicable to DXD4 clad. Furthermore, because the alloy composition is covered by the fatigue-tested Zircaloy-2, Zircaloy-3, and Zircaloy-4 alloys, the same fatigue criterion is applicable. Any small variations in properties and behavior relative to through-wall Zircaloy-4 are accommodated by the conservatism in the 0.67 fatigue usage design limit.

#### 4.1.4 Fretting Wear

SPC's design basis for fretting corrosion and wear specifies that fuel rod failures due to fretting shall not occur (Reference 1, Section 3.3.3). Fretting wear depends chiefly on spacer grid and rod retention system design features, and on the hydraulic environment in which the fuel rod operates.

Because significant amounts of fretting wear can eventually lead to fuel rod failure, spacer grid assemblies are designed to prevent such wear. In addition, Siemens performs fretting tests to verify consistent fretting performance for new spacer designs. Examination of a large number of irradiated rods has substantiated the appropriateness of the fretting tests.

Based on its similar metal content and treatment in the cladding production process, as well as the results of post-irradiation fuel rod inspections, Siemens expects DXD4 cladding to exhibit the same fretting wear behavior as Zircaloy-4 cladding. Full-length visual inspection of five DXD4 fuel rods irradiated to burnups of 44 to 45 MWd/kgU revealed no indications of fretting wear, confirming these expectations. Therefore, the SPC design basis for fretting wear is considered applicable to both DXD4 cladding and Zircaloy-4 cladding. SPC will continue to apply its approved mechanical design methods for fretting wear to fuel with DXD4 cladding.

#### 4.1.5 Oxidation, Hydrogen Pick-up, and Crud Buildup

SPC has carefully investigated, through post-irradiation poolside and hot-cell examinations, the oxidation, or corrosion, of DXD4 cladding under typical PWR operating conditions. Results of these investigations show that the corrosion behavior of DXD4 cladding is significantly superior to that of Zircaloy-4 cladding. A complete analysis of DXD4 cladding corrosion behavior, as well as the description of a newly developed corrosion model used to predict cladding oxide thickness as a function of power history and burnup, are provided in Appendix B. A summary of the important observations and conclusions is provided here.

DXD4 cladding corrosion behavior was measured in five PWRs, four in Europe and one in the U.S. The measured oxide thickness, represented as the maximum running-average

thickness of the corrosion layer on a fuel rod, is shown as a function of burnup in Figure 4.1.5.1. Data were collected during multiple, consecutive reactor cycles, and include corrosion data for fuel with a rod-average burnup of approximately [ ] MWd/kgU in a plant with very demanding operating conditions (core average LHGR: 229 W/cm, coolant temperature: 309°C). The maximum oxide thickness measured was [ ] microns; no spalling of oxide was observed on any fuel rod with DXD4 cladding.

SPC's currently approved design basis for corrosion of fuel rods specifies that the rod "peak" oxide thickness shall not exceed [ ] microns on a 95/95 basis. This differs from the typical industry criterion, as the limit applies to measurements made on a "peak local" basis, and because the data have been processed to develop a 95/95 statistical bound. The DXD4 fuel rod oxide thickness measurements presented in this report were made using maximum-running-average and circumferential-average techniques; these techniques are consistent with industry practice. Benchmarking these averaging techniques to the peak-local-basis technique showed that the averaging techniques produce measurements that are about 91% of those made using the peak-local-basis technique. The [ ] criterion of the peak-local-basis technique was therefore adjusted to [

]. Oxide thickness will continue to be evaluated on a 95/95 basis, and this adjusted limit preserves the conservatism in the oxide thickness evaluation. DXD4 cladding meets this corrosion criterion by a wide margin up to the requested burnup of 62 MWd/kgU, under even the most demanding circumstances.

The oxide thickness data were used to develop and benchmark a corrosion model that incorporates a second-transition corrosion rate increase. This model accounts for the increase in corrosion rate that is observed at an oxide thickness of approximately [

] microns. The new model, called CORROS II, is incorporated into SPC's approved fuel performance code and calculates best-estimate and 95/95 maximum running-average values of fuel rod oxide thickness as a function of burnup for a defined power history and defined plant operating conditions. The analyses in Appendix B show that the corrosion behavior of DXD4 cladding is accurately predicted by CORROS II up to at least [ ] MWd/kgU when the following parameters are used:

[

]

A comparison of calculated oxide thickness values with measured values is shown in Figure 4.1.5.2. The predicted oxide thickness as a function of burnup for one PWR (Plant D24) is shown in Figure 4.1.5.3.



**Figure 4.1.5.1 DXD4 Cladding Oxide Thickness as a Function of Burnup**



**Figure 4.1.5.2** Comparison of Measured and CORROS II-Calculated Oxide  
for Five PWR Plants





**Figure 4.1.5.4** Hydrogen Pick-up as a Function of Oxide Thickness

#### 4.1.6 Rod Bowing

Differential expansion between fuel rods and guide tubes, as well as lateral thermal and flux gradients, can lead to lateral creep rod bow in the spans between spacer grids. This lateral creep bow changes rod-rod gaps in the span between spacer grids and may affect the peaking and local heat transfer. The SPC design basis for fuel rod bowing specifies that lateral displacement of the fuel rods shall be sufficiently small that it does not impact thermal margins (Reference 1, Section 3.3.5).

To evaluate the effect of rod bow on thermal margins, SPC uses a conservative rod bow projection which is linear with burnup. Extensive post-irradiation inspections of Zircaloy-4 fuel assemblies have confirmed that rod bow has not reduced spacing between adjacent rods by more than [     ]. The potential effect of greater bow on thermal margins is negligible because of the lower power achieved at high exposure.

No change in rod bow behavior is expected for DXD4 clad fuel rods, as the bulk of the clad is Zircaloy-4 – the reference material – and because no unusual rod bow has been noted in

Duplex D4 (DXD4) Cladding for PWRs

the approximately 580,000 Duplex rods (2,311 PWR fuel assemblies) that have been irradiated.

#### 4.1.7 Axial Growth

The PWR fuel assembly axial growth design criteria specify that clearance between the upper and lower tie plates and the fuel rods shall be maintained for all fuel rods during their design life, and the clearance between the tie plates and the reactor core plates shall be maintained during the assembly's design lifetime (Reference 1, Section 3.3.6). These criteria are established so that rod bow remains predictable and assembly bow that could impede control rod insertion does not occur.

Because the bulk inner layer of DXD4 cladding is Zircaloy-4, irradiation-induced axial growth similar to that observed in Zircaloy-4 cladding is expected. Growth data for DXD4 cladding have been collected at four reactors, to rod burnups of [ ] MWd/kgU. The DXD4 growth shows a lower trend than standard Zircaloy-4, but quite similar to [ ].

Figure 4.1.7.1 shows the predicted and 95/95 upper-bound rod growth for Optimized Zircaloy-4 cladding, compared to the approved upper-bound design curve for all SPC PWR cladding growth, including standard Zircaloy-4. The upper bound for the Optimized Zircaloy-4 data shows about a [ ] from the reference Zircaloy-4 upper bound.

Axial growth data for DXD4 rods are shown in Figure 4.1.7.2. The predicted growth and upper bound are also reduced relative to the reference Zircaloy-4 design curve; the [ ].

Figure 4.1.7.3 shows the combined Optimized Zircaloy-4 and DXD4 growth results. This curve shows about a [ ] improvement relative to standard Zircaloy-4, and is conservative relative to the high-burnup DXD4 data.

The combined data set for DXD4 and Optimized Zircaloy-4 cladding provides both high-burnup projections based on the DXD4 data, and greater statistical experience with different cladding lots and reactor applications for the Optimized Zircaloy-4 data. The

95/95 upper bound shown for the combined Optimized Zircaloy-4 and DXD4 data will therefore be used for evaluating DXD4 growth until more DXD4 data become available. Fuel rod design margins for growth will be improved with the introduction of DXD4.

Because the DXD4 tubing is used for fuel rod cladding and not guide tubes, DXD4 cladding has no effect on assembly growth. Also, because the maximum projected growth is lower for the DXD4 clad than for standard Zircaloy-4, any influence of rod growth on assembly growth due to frictional interaction between the rods and the assembly will be reduced with the introduction of DXD4 cladding. The existing fuel assembly growth models will therefore be conservative.



**Figure 4.1.7.1** Optimized Zircaloy-4 Fuel Rod Growth as a Function of Fast Fluence



**Figure 4.1.7.2 Duplex D4 Fuel Rod Growth as a Function of Fast Fluence**



**Figure 4.1.7.3 Comparison of Optimized Zircaloy-4 and Duplex D4 Fuel Rod Growth as a Function of Fast Fluence**

#### 4.1.8 Rod Internal Pressure

Rod internal pressure is a driving force for, rather than a direct mechanism of, fuel system damage that could contribute to the loss of dimensional stability and cladding integrity. To preclude fuel damage, SPC limits the calculated rod internal gas pressure to system pressure plus [ ] psi (Reference 1, Section 3.3.7).

The two concerns of internal rod pressures exceeding system pressures during normal operations are: 1) zircaloy cladding could creep away from the fuel, resulting in a larger gap, lower fuel-cladding gap conductivity, and higher temperatures and fission gas release (i.e., a thermal feedback effect); and 2) hydride reorientation within the zircaloy cladding that could result in loss of ductility and the subsequent possibility of brittle fracture.

Fuel rod internal pressure is calculated with the RODEX2 code. The RODEX2 code pressure predictions are dependent on the fuel and clad thermal properties, the void volume in the rod, and the state of the pellet-clad gap.

The fuel properties for rods with DXD4 cladding are the same as those for through-wall Zircaloy-4 clad rods. Likewise, because DXD4 cladding is essentially a zircaloy-type alloy with small composition differences in the outer layer, the thermal conductivities of Zircaloy-4 and DXD4 claddings are the same (see Section 7.2.3).

Nominal clad axial growth, which affects the length of the plenum, is essentially the same for DXD4 cladding as for Optimized Zircaloy-4 (see Section 4.1.7). This growth is also approximately equal to the nominal growth used in the RODEX2 benchmarking. Therefore, calculated void volumes in both types of rods are the same.

The prediction of pellet-clad gap is dependent on the clad creepdown. A comparison of the RODEX2-calculated creepdown and measured data for rods with Duplex cladding, shown in Figure 4.1.2.1, shows that the code predictions match the measured data well. As discussed in Appendix A, the clad thermal creep component may be increased due to the lower creep strength of the Duplex layer. The theoretical overall clad thermal creep, and thus the overall thermal-plus-irradiation creepdown of DXD4 cladding, could be slightly increased relative to through-wall Zircaloy-4 cladding, resulting in an overall smaller pellet-

clad gap than for equivalent through-wall cladding. This would tend to produce very slightly lower clad temperatures, gas release, and resulting rod pressure.

RODEX2 has been shown to be applicable for calculating internal pressure of rods with Duplex cladding, based on equal fuel properties and equivalent or conservative clad properties. The existing methods for evaluating the margin to the fuel rod pressure limit with the RODEX2 code will be retained.

DXD4 cladding has a lower corrosion rate than Zircaloy-4 clad and [

] (see Section 4.1.5).

This results in lower hydrogen concentrations in DXD4 cladding than in Zircaloy-4 clad for the same reactor duty. The pressure stresses in DXD4 clad will be the same as those in Zircaloy-4 cladding for the same operational conditions. Because the same design pressure criterion [ ] is chosen for the DXD4 clad fuel rods, the limiting hydride reorientation behavior will be the same as for Zircaloy-4, conservatively neglecting any benefit resulting from the overall lower hydrogen concentrations in DXD4.

The internal pressure calculation methodology and design criterion limit used for Zircaloy-4 are therefore applicable for DXD4 cladding.

#### 4.1.9 Assembly Liftoff

The SPC design criterion for assembly liftoff specifies that the assembly shall not levitate from hydraulic loads (Reference 1, Section 3.3.8). Therefore, for normal operation and anticipated operational occurrences (AOOs), the submerged fuel assembly weight and hold-down must be greater than the upward hydraulic loads.

DXD4 cladding has no impact on this criterion other than through its weight. Because the weight difference between DXD4 and Zircaloy-4 cladding is negligible, replacing Zircaloy-4 cladding with DXD4 cladding of the same thickness will have no impact on assembly liftoff. Weight changes that would occur due to changes in cladding thickness will be addressed with normal revisions to the liftoff calculations.

#### 4.1.10 Control Rod Reactivity

SPC's design basis for the fuel assembly specifies that the Technical Specification shutdown margin will be maintained (Reference 1, Section 5.2). Specifically, the assemblies and core must be designed to remain subcritical with the highest-reactivity-worth control rod fully withdrawn and the remaining control rods fully inserted. Shutdown margin is calculated and demonstrated at the beginning of the cycle (as a minimum) for each reactor. SPC uses standard approved design methods to ensure that adequate limits are placed on control rod worth.

A slight increase in [

] in the D4 alloy will tend to increase the neutron absorption cross-section of the D4 metal compared to Zircaloy-4. D4 material constitutes only a fraction of the total DXD4 cladding mass, and the remaining material is Zircaloy-4. Therefore, the effective change in cross-section between claddings of Zircaloy-4 and DXD4 is small. SPC will continue to use approved design methods in the determination of control rod reactivity, treating DXD4 cladding as Zircaloy-4.

### 4.2 ***Fuel Rod Failure***

#### 4.2.1 Hydriding (Internal)

SPC reduces the potential for hydrogen absorption on the inside of the cladding by eliminating potential sources of moisture during fuel rod fabrication, including the careful control of fuel pellet moisture content. By controlling the moisture content of the fuel pellets, the fabrication limit for total hydrogen inside the fuel rod is maintained at a minimal level (Reference 1, Section 3.2.1).

The absorption of hydrogen by fuel rod cladding can result in cladding failure due to reduced ductility and the formation of hydride platelets. Cladding type does not affect the internal hydrogen content in a fuel rod, and because the inner wall of DXD4 cladding is Zircaloy-4, the effect of hydrogen on the cladding inner surface is the same for DXD4 cladding as for Zircaloy-4 cladding.

To verify that acceptably low levels of hydrogen are being maintained, a statistical sample of fabricated pellets is selected for analysis, and the hydrogen content is measured and compared to the established limit. SPC has experienced no significant level of fuel failures due to internal hydriding, confirming that the testing and sampling processes permit adequate control of moisture within the fuel rods. SPC will continue its current practice for controlling internal hydrogen concentration; for the reasons stated above, internal hydriding experience with DXD4 cladding is expected to be the same as for Zircaloy-4 cladding.

#### 4.2.2 Cladding Collapse

The SPC cladding creep collapse criterion is designed to prevent the formation of significant axial gaps in the fuel pellet column due to pellet densification (Reference 1, Section 3.2.2). The opening of axial gaps in the pellet column creates the potential for cladding to collapse (flatten) into the gap, where the large local strains resulting from cladding collapse could be sufficient to cause clad failure. Thus, the cladding creep collapse criterion is established to preclude cladding collapse during the design lives of fuel rods and burnable absorber rods.

The methodology used to demonstrate compliance with the cladding creep collapse criterion determines whether pellet hang-up can occur during the [

]. The collapse criterion specifies that cladding uniform creepdown (calculated with RODEX2), combined with an ovality increase (calculated with COLAPX), shall not cause the pellets to become locked-up inside the cladding. If the pellets are free to move axially, the pellet column can consolidate due to densification and, under the force of the fuel rod plenum spring, prevent the formation of axial gaps. SPC's collapse criterion requires that the cladding inner diameter decrease due to the combined effects of cladding creepdown and ovality increase [ ] be less than the initial minimum diametrical gap. This approach conservatively neglects pellet densification.

Both uniform creepdown and ovality increase, which are combined together to evaluate the degree of diametrical gap closure, are controlled by the creep strain rate of the cladding. As discussed in Section 4.1.2, the thermal creep strain rate of DXD4 cladding can be

slightly higher than that of standard through-wall Zircaloy-4 cladding. It is, however, within the upper end of the scatter band of thermal creep strain rate data for through-wall Optimized Zircaloy-4 cladding (see Table A.1 in Appendix A). After a significant period of irradiation, thermal creep is the minor component of the total creep strain, contributing [ ]. However, the relative contribution of thermal creep to total creep strain is important early in a fuel rod's irradiation life, accounting for as much as [ ]. Thus, it is estimated that the total creep strain of DXD4 clad at [

]. This minor difference is accommodated by the high degree of conservatism in the analysis of the cladding creep collapse criterion.

Figure 4.2.2.1 shows the diameter profile, based on a helical scan, of a DXD4 fuel rod after [ ]; the width of the trace at any axial location along the rod represents cladding ovality. Cladding creepdown for this rod is shown in Figure 4.1.2.1. Maximum cladding ovality for this one-cycle fuel rod is [ ] at a burnup approximately three times that considered in the cladding creep collapse analysis. This indicates that [ ].

These results show that the analysis is conservative and that the methodology used for through-wall cladding can be used for DXD4 cladding.



**Figure 4.2.2.1 Helical Diameter Scan of a One-Cycle DXD4 Fuel Rod**

#### 4.2.3 Overheating of Cladding

The design basis to preclude fuel rod cladding overheating specifies that there must be at least 95% probability at a 95% confidence level that any fuel rod in the core does not experience departure from nucleate boiling (DNB) during steady-state operation and anticipated operational occurrences (Reference 1, Section 3.2.3).

##### Effect of DXD4 Cladding on DNB Phenomena

Overheating of the cladding occurs when there is a sharp reduction in the surface heat transfer coefficient, caused by the formation of an insulating vapor layer on the cladding surface. This phenomenon is commonly called departure from nucleate boiling, or DNB. The parameters that dominate the heat flux at which DNB occurs include: 1) the mechanical design of the fuel assembly, in particular, the spacer grid which is designed to strip the vapor layer from the cladding surface; and 2) the fluid conditions, such as mass flux, pressure, and quality. The cladding material and its thermal conductivity and heat capacity have no significant effect on the surface heat transfer coefficient and surface heat flux at which DNB occurs. When a vapor layer exists on the cladding surface, the fuel rod is not conduction-limited and the rod heat flux is dominated by the surface heat transfer

coefficient. Therefore, there is no significant effect of either DXD4 cladding or Zircaloy-4 cladding on DNB phenomena.

#### Effect of DXD4 Cladding on DNBR Criterion

Fuel cladding integrity is maintained by ensuring that the minimum DNBR remains above the 95/95 DNB correlation limit for a given fuel design. The 95/95 DNB correlation limit is derived from DNB test data. As indicated above, neither DXD4 nor Zircaloy-4 cladding has a significant effect on DNB phenomena. Thus, fuel assemblies are typically simulated by Inconel clad heater rods in DNB tests. Therefore, use of DXD4 cladding will have no effect on the DNB data or the DNBR criterion (95/95 DNB correlation limit).

#### 4.2.4 Overheating of Fuel Pellets

The design criterion for overheating of fuel pellets specifies that the centerline temperature of the fuel pellets must remain below the pellet melting temperature during normal operation and anticipated operational occurrences (Reference 1, Section 3.2.4).

The centerline melting criterion was established to assure that axial or radial relocation of molten fuel would neither allow molten fuel to come into contact with the cladding nor produce local hot spots. For normal operation and anticipated operational occurrences, centerline melting is not permitted. In calculations of radiological dose for the case of postulated accidents, all rods that experience centerline melting are assumed to fail. This assumption that centerline melting results in fuel failure is conservative.

The margin to centerline melting is calculated with the RODEX2 code, in which predictions of fuel temperature are dependent on linear heat rate, the fuel properties, the state of the pellet-clad gap, and the thermal conductivity of the clad. As stated in Section 4.1.8, the fuel properties for rods with DXD4 cladding are the same as those for through-wall Zircaloy-4 clad rods, and because DXD4 cladding consists of a Zircaloy-4 base material with a thin outer layer of D4 alloy (essentially Zircaloy-type material with small composition variations), Zircaloy-4 and DXD4 claddings exhibit the same thermal conductivity (see Section 7.2.3).

The prediction of pellet-clad gap depends on the clad creepdown. Comparison of RODEX2-calculated creepdown to measured data for rods with DXD4 cladding (see Figure 4.1.2.1) shows a good match between the code predictions and measured data. As discussed in Section 4.1.2, the clad thermal creep component may be increased due to the lower creep strength of the Duplex layer. As a result, the theoretical overall clad thermal creep, and thus the overall thermal-plus-irradiation creepdown, could be slightly greater for Duplex cladding than for through-wall cladding, resulting in an overall smaller pellet-clad gap in Duplex rods than in rods with through-wall cladding. This would result in better heat transfer out of the rod and lower centerline temperatures.

RODEX2 has been shown to be applicable for calculating fuel temperatures for Duplex clad rods that have equal fuel properties and equivalent or conservative clad properties relative to through-wall clad rods. Therefore, the existing methods for evaluating the margin to fuel melting with the RODEX2 code will be retained. Substituting DXD4 cladding for Zircaloy-4 will not result in any revision to analyses for overheating of fuel pellets.

#### 4.2.5 Pellet-Cladding Interaction

The Standard Review Plan does not contain explicit criteria to address pellet-cladding interaction; however, it does present three related criteria:

1. The uniform strain of the cladding should not exceed 1%. In this context, uniform strain (elastic and inelastic) is defined as transient-induced deformation with gage lengths corresponding to cladding dimensions.
2. Fuel melting should be avoided. The large volume increase associated with melting may cause a pellet with a molten center to exert a stress on the cladding.
3. Clad fatigue usage shall be limited. Cyclic loading associated with relatively large changes in power can cause cumulative damage which may eventually lead to fatigue failure. SPC uses a conservative fatigue usage limit of 0.67.

These criteria and the methodology to address them are unaffected by the change from through-wall Zircaloy-4 to Duplex cladding with a Zircaloy-4 wall and D4 alloy outer layer,

and are addressed in Sections 4.1.2 "Design Strain," 4.1.3 "Strain Fatigue," and 4.2.4 "Overheating Of Fuel Pellets."

#### 4.2.6 Cladding Rupture and Ballooning

To meet the requirements of 10 CFR 50.46 as it relates to ECCS performance evaluation, as well as those of 10 CFR Part 50, Appendix K, as it relates to the incidence of rupture during a LOCA, Siemens has performed appropriate tests of DXD4 cladding to show that it behaves the same as or better than Zircaloy-4 cladding. In future evaluations, fuel with DXD4 cladding will, therefore, be evaluated using the well-established material properties of Zircaloy-4.

The stress rupture tests conducted by Siemens indicate that the time to failure of DXD4 and other Duplex cladding variants is the same as that of Zircaloy-4 cladding when tested under the same conditions. Test results are shown in Figure 4.2.6.1. A detailed description of the tests, a complete compilation of the test results, and an analysis of the results are presented in Appendix D. The results indicate that neither the Duplex fabrication process nor the small variation in alloy content of either the Zircaloy-4 or Duplex layer results in significantly different time-to-rupture behavior.

The ballooning and rupture hoop strain behavior of DXD4 cladding, as determined in the stress rupture tests, is shown in Figure 4.2.6.2. As shown in the figure, the maximum strain observed in DXD4 cladding does not exceed the bounding maximum hoop strain of the Zircaloy-4 cladding reference material. This result is fully within expectations, as the average tin content of DXD4 cladding falls within the specification range for Optimized Zircaloy-4 cladding. A complete discussion of the stress rupture tests is presented in Appendix D.



**Figure 4.2.6.1** Time to Rupture of DXD4 and DXB Cladding as a Function of Temperature and Initial Cladding Hoop Stress



**Figure 4.2.6.2** Rupture Hoop Strain of DXD4 and DXB Cladding Compared to the Standard Zircaloy-4 Cladding Reference Maximum Hoop Strain

#### 4.2.7 Fuel Rod Mechanical Fracturing

A mechanical fracture refers to a defect in a fuel rod caused by an externally applied force. SPC limits the combined stresses from postulated accidents to the stress limits given in ASME Code Section III, Appendix F, for faulted conditions (Reference 1, Section 3.2.7). Cladding integrity is determined to be maintained if the applied stress is less than 90% of the irradiated yield stress at the appropriate temperature. The beginning-of-life yield strength is used as a conservative lower bound on the irradiated cladding yield strength.

The material properties of the DXD4 cladding (yield strength, ultimate strength, ductility, and burst test properties) are specified on the same basis as those of through-wall Zircaloy-4 cladding. The current DXD4 specification [

].

Accident stresses may include axial, circumferential, and axial bending components. As discussed in Section 4.1.1, the axial and circumferential stresses of Duplex cladding can be evaluated on the same basis [ ] as specified for through-wall cladding. Axial bending can also be evaluated using the through-wall specification basis, because the clad can be assumed to be two concentric cylinders whose bending properties are essentially additive, as the tubes are approximately the same diameter. DXD4 cladding will therefore be evaluated [ ] as through-wall Zircaloy-4 cladding, developed on the same basis as for design stress (Section 4.1.1).

#### 4.2.8 Excessive Enthalpy

For PWR severe reactivity-initiated accidents (e.g., CEA ejection), the 95/95 DNB correlation limit is used as the fuel failure criterion. As discussed in Section 4.2.3, DXD4 cladding has no significant effect on the DNB phenomena, DNB test data, or DNBR criterion (95/95 DNB correlation limit). Additional discussion relating to reactivity-initiated accidents is provided in Section 4.3.2 "Violent Expulsion of Fuel."

### 4.3 *Fuel Coolability*

#### 4.3.1 Fragmentation of Embrittled Cladding

The criteria for fragmentation of embrittled cladding as related to LOCA evaluations are stated in 10 CFR 50.46 as: 1) the fuel rod cladding temperature shall remain less than 2200 °F, and 2) the maximum oxidation of the cladding shall remain less than 17% equivalent cladding reacted (ECR).

Siemens has conducted appropriate high-temperature steam corrosion and quench tests of DXD4 cladding and compared the results with similar tests performed on Zircaloy-4 reference cladding. The test results show comparable weight gains and levels of oxygen penetration for Zircaloy-4 and DXD4 cladding during high-temperature oxidation in saturated steam at temperatures up to 1250°C. Quench behavior of the two materials was also found to be the same. A full description of the tests and a discussion of the test results are presented in Appendix E.

A comparison of the corrosion-caused weight gain as a function of time for DXD4 cladding and Zircaloy-4 reference cladding is shown in Figure 4.3.1.1. This figure shows that the high-temperature steam corrosion behavior of DXD4 cladding is conservatively described by equations appropriate for Zircaloy-4, as the high-temperature corrosion weight gain of DXD4 cladding is slightly less than the weight gain of Zircaloy-4 reference cladding.

Representative metallographic sections of the rapidly quenched high-temperature corrosion test samples, shown in Figures 4.3.1.2 through 4.3.1.4 and other figures in Appendix E, show that the diffusion of oxygen into the cladding wall is the same for DXD4 and Zircaloy-4 cladding. The oxygen-stabilized alpha layer in both types of cladding is severely embrittled and is fractured after quenching. The fracture cracks appear as white lines in the alpha-stabilized layer in the metallographs. The high-temperature steam corrosion and quench tests indicate that corrosion of up to 25% equivalent cladding reacted does not lead to cladding failure upon rapid quenching; therefore, the "2200°F" and "17% ECR" criteria, as specified in CFR 50.46, can be applied to DXD4 cladding in the same manner as it is applied to Zircaloy-4 cladding.



**Figure 4.3.1.1** Comparison of Weight Gain as a Function of Time  
for Through-Wall Zircaloy-4 and Duplex D4 Cladding



**Figure 4.3.1.2 Duplex D4 Cladding Exposed for One (1) Minute at 1050°C**



**Figure 4.3.1.3** Through-Wall Zircaloy-4 Cladding Exposed for Ten (10) Minutes at 1050°C

Duplex D4 (DXD4) Cladding for PWRs

---



**Figure 4.3.1.4 Duplex D4 Cladding Exposed for Ten (10) Minutes at 1250°C**

#### 4.3.2 Violent Expulsion of Fuel

The SPC design criterion for violent expulsion of fuel limits the deposited enthalpy to less than 280 cal/g (Reference 1, Section 3.4.2).

In severe reactivity-initiated accidents, such as control rod ejection in a PWR or control rod drop in a BWR, the large and rapid deposition of energy in the fuel can result in melting, fragmentation, and dispersal of fuel. The mechanical action associated with fuel dispersal can be sufficient to destroy the cladding and the rod-bundle geometry of the fuel, and can produce pressure pulses in the primary system. To meet the guidelines of Regulatory Guide 1.77 as it relates to preventing widespread fragmentation and dispersal of the fuel and avoiding the generation of pressure pulses in the primary system of a PWR, a radially averaged enthalpy limit of 1.17 kJ/g (280 cal/g) should be observed. The minor differences in chemical composition and mechanical properties between through-wall Zircaloy-4 cladding and DXD4 cladding have little, if any, effect on radially averaged enthalpy. Therefore, the use of this criterion for fuel with DXD4 cladding is acceptable.

The issue of the appropriate criteria for reactivity-initiated accidents is currently being considered by both the nuclear industry and the NRC. A number of recent tests indicate that the 280 cal/g enthalpy criterion may be nonconservative and that the state of the cladding may influence fuel rod failures. In particular, recent tests indicate that cladding with high corrosion levels may be more prone to failure. In this context, the use of DXD4 cladding, with its significantly lower corrosion levels, is beneficial.

The NRC position relative to these criteria was stated in the Safety Evaluation Report for Reference 1:

*The staff has reviewed the enclosed TER, and concludes that the TER provides adequate technical basis to approve EMF-92-116(P), except for Section 3.2, Violent Expulsion of Fuel. With regard to Section 3.2, the staff believes that additional clarification is necessary with respect to the acceptance criteria in Regulatory Guide 1.77 and Standard Review Plan 4.2 for rod ejection accidents. These acceptance criteria are considered nonconservative in light of some test data from foreign test reactors on reactivity-initiated accidents. However, the staff considers the fuel to be acceptable to a rod-average burnup level of 62 GWd/MTU burnup because the probability of these accidents is low and generic plant transient*

*calculations indicate that energy inputs during these transients are low and will remain below the relevant test data failure levels. This position is consistent with the Agency Program Plan for High-Burnup Fuel and the memorandum from L. Callan to the Commissioners dated July 15, 1997.*

*With this clarification, the staff agrees with PNNL's conclusion that the fuel mechanical design criteria described in EMF-92-116(P) are acceptable for PWR licensing applications. Based on our review, the staff adopts the findings in the attached TER.*

#### 4.3.3 Cladding Ballooning

Cladding ballooning is discussed in Section 4.2.6, "Cladding Rupture and Ballooning."

#### 4.3.4 Fuel Assembly Structural Damage from External Forces

Earthquakes and postulated pipe breaks in the reactor coolant system can result in external forces on the fuel assembly. The Standard Review Plan Section 4.2 and the associated Appendix A state that fuel system coolability should be maintained and damage should not be severe enough to prevent control rod insertion, when required, during these low-probability accidents. The SPC design criteria are consistent with the SRP (Reference 1, Section 3.3).

Fuel system coolability and the ability to insert control rods are determined by the fuel assembly structure, in particular the geometry of the spacer grids and guide tubes. Irrespective of fuel rod cladding material, spacer grids and guide tubes will be made of Zircaloy-4; therefore, no change in the method for evaluating fuel system coolability and the ability to insert control rods is required. The use of DXD4 to replace Zircaloy-4 cladding will have no impact on this criterion.

The elastic modulus of DXD4 cladding is the same as that of Zircaloy-4. Therefore, structural loads determined for fuel assemblies with Zircaloy-4 cladding fuel rods will remain applicable to assemblies with the same structure but containing DXD4 fuel rod cladding.

(This page was intentionally left blank.)

## 5.0 Design Analysis

### 5.1 Introduction

For the example fuel rod design analyses presented here, SPC re-performed fuel rod analyses for a current SPC PWR reload design case which produced the most-limiting calculation results for Optimized (low-tin) Zircaloy-4 cladding. The analyses were performed by substituting DXD4 cladding corrosion and growth properties, and adjusting methodologies (described earlier in this report), as appropriate. The current SPC PWR reload design case which produced the most-limiting calculation results is based on SPC's advanced 17x17 fuel assembly design. The calculations show that the design criteria are satisfied for DXD4 clad fuel rods, and that DXD4 corrosion and rod growth predictions show significant improvement over those for Zircaloy-4.

### 5.2 Description of Fuel Design Analyses

The fuel rod design analyses consist of a group of calculations that use the NRC-approved RODEX2 code, in addition to other support codes. The following subsections describe the fuel design calculations which are affected by differences in properties between Zircaloy-4 and DXD4 claddings.

#### 5.2.1 Cladding Collapse

During initial fuel densification, axial gaps may form within the fuel column. Consequently, a cladding creep analysis is performed to verify that the pellet-cladding gap does not close [ ]. Cladding creep calculations were performed according to NRC-approved methodology (Reference 7).

The fuel rod plenum spring was designed to help preclude cladding collapse by ensuring that sufficient axial force is applied to the fuel stack to help prevent the formation of axial gaps in the pellet stack during shipping, handling, and operation of the fuel. The spring can accommodate stack length variations due to initial fuel densification of [ ]. Furthermore, the pitch of the spring is designed, using stiffening ring relationships, to prevent collapse in the upper plenum region of the fuel rod.

Because the plenum spring design is the same for fuel rods with Zircaloy-4 and DXD4 cladding, spring design calculations were not repeated. Previous SPC analyses have verified that the pellet-cladding gap remains open through completion of fuel densification. This analysis result will remain unchanged for DXD4 clad rods, as the effect of cladding corrosion on fuel rod temperature (favorable for DXD4), and therefore fuel rod pressure and cladding strain, is negligible during the densification phase of the fuel.

### 5.2.2 Overheating of Fuel Pellets

To verify that the fuel pellets will not overheat, the fuel rod design is analyzed to show that pellet centerline melting does not occur during normal operations or anticipated operational occurrences (AOOs). The analysis for DXD4 cladding differs from that for Zircaloy-4 cladding only in the effect of reduced cladding corrosion on rod temperature. As stated before, the effect is very small, and no change in pellet centerline melting behavior is expected.

### 5.2.3 Pellet-Cladding Interaction

To determine the stresses and strains during transients, ramps to maximum linear heat generation rate (LHGR) conditions were added to the steady-state power histories. Ramp power levels were determined by applying the following conservative factor to the local power levels periodically throughout irradiation:



The initial conditions for the transients are obtained from RODEX2 code output. Ramps that simulate the startup from a cold shutdown were held at the terminal power for 24 hours. A partial filling of the pellet-clad gap with a pellet chip was also assumed at each reactor startup. The same ramp rates were used for Zircaloy-4 and DXD4 analyses. This

Duplex D4 (DXD4) Cladding for PWRs

analysis for DXD4 cladding differs from that for Zircaloy-4 cladding only in the very small effect of reduced cladding corrosion on fuel rod temperature.

#### 5.2.4 Cladding Stresses

The steady-state cladding stress analysis was performed considering the stress relationships described in Reference 8. These relationships consider primary and secondary membrane and bending stresses due to hydrostatic pressure, flow-induced vibration, ovality, spacer contact, pellet-cladding interaction, thermal and mechanical bow, and thermal gradients. Stresses were calculated for all combinations of the following conditions and locations:

- Beginning-of-life (BOL) and end-of-life (EOL)
- Cold and hot conditions
- At mid-span and at spacer locations
- At both the inner and outer surfaces of the cladding

The applicable stresses in each orthogonal direction were combined to calculate the maximum stress intensities, which were then compared to the applicable ASME Code design criteria given in Reference 1. As above, this analysis for DXD4 cladding differs from that for Zircaloy-4 cladding only in the very small effect of reduced cladding corrosion on fuel rod temperature.

#### 5.2.5 Cladding Strain

In addition to the ramping analysis described above, cladding strain was analyzed in both steady-state conditions and under simulated AOOs. For steady-state conditions, the strain analyses were performed with the RODEX2 code and the design power histories. The creep strain at any time throughout the fuel life was compared to the 1.0% circumferential strain criterion. Simulated AOOs were evaluated to determine the cladding total uniform strain that would occur if a rod was at the maximum allowable power peaking levels. A local power factor [

] was applied periodically throughout irradiation. Use of

Duplex D4 (DXD4) Cladding for PWRs

---

DXD4 cladding affects this analysis only in the very small change of reduced clad corrosion on rod temperature.

#### 5.2.6 Fatigue

The stresses calculated in the ramping analysis (see above) were used to evaluate cladding fatigue damage through EOL due to cyclic power variations. For conservatism, all cycles were considered to cause the extreme maximum stresses for the fatigue evaluation.

The transient stress results were evaluated to determine the fatigue usage for each cycle based on the O'Donnell and Langer design curve (Reference 6). These results were accumulated to determine the total fatigue usage factor. As with other analyses, use of DXD4 cladding affects this analysis only in the very small change of reduced clad corrosion on rod temperature.

#### 5.2.7 Oxidation, Hydriding, and Crud Buildup

External corrosion is calculated for Optimized Zircaloy-4 cladding using the MATPRO model, and for DXD4 cladding using the second-transition corrosion model described in Section 4.1.5 and Appendix B. The fuel rod corrosion analysis for the reference case for Optimized Zircaloy-4 takes into account the methodology updates that resulted from the NRC's review and approval of Reference 1. The analysis for DXD4 uses the new design corrosion equation presented in Section 4.1.5 and Appendix B, which projects reduced corrosion for DXD4 cladding relative to Zircaloy-4.

#### 5.2.8 Fuel Rod Growth

Projected fuel rod growth behavior is based on measured data collected during poolside fuel examinations. The maximum predicted EOL rod growth is calculated using the maximum growth curve based on these data. Conservative temperatures, worst-case dimensional clearances, maximum rod growth, and minimum assembly growth are used in the analysis.

The fuel rod growth analysis takes into account the methodology resulting from the NRC's review and approval of Reference 1. For conservatism, the bounding growth correlation

for [ ] is used in fuel rod design analyses.

### 5.2.9 Rod Internal Pressure

Calculation of fuel rod internal pressure is performed with the RODEX2 code. Power histories for the gas pressure analysis were developed from the corresponding power histories in accordance with NRC-approved methodology (Reference 7). For cases where system pressure is exceeded, the pellet-cladding gap does not increase during steady or increasing power conditions. This analysis differs for DXD4 cladding only due to the very small effect of reduced clad corrosion on fuel rod temperature.

### 5.3 *Results of Fuel Design Analysis*

The second-transition corrosion model developed for DXD4 cladding (Section 4.1.5) has been incorporated into the RODEX2 computer code. Although no changes were needed for the cladding stress, strain, internal pressure, or collapse models, the modified RODEX2 corrosion model may have some effects on temperature and other temperature-dependent calculation results. Therefore, SPC has performed a complete fuel rod design analysis. Results of the design analysis are summarized in Table 5.1; corresponding results for Zircaloy-4 cladding are shown for comparison.

Fuel rod power histories for the most-limiting gas pressure and corrosion cases are shown in Figure 5.1. Figure 5.2 shows power histories for the most-limiting rods for fatigue, collapse, AOO strain, and steady-state strain. Data for both urania and urania/gadolinia rods are shown in the figures.

Oxide thickness predictions for the most-limiting urania and urania/gadolinia DXD4 rods are shown in Figure 5.3. Both best-fit and 95/95 upper-bound oxide thickness curves are presented. DXD4 rod internal pressure predictions for the most-limiting urania and urania/gadolinia rods are shown in Figure 5.4.

#### 5.4 ***Conclusions***

SPC has performed an example DXD4 fuel rod design analysis using the most-limiting design case for current SPC methodology. The calculation results show that the design criteria were satisfied. Compatible results for fatigue, stress, strain, collapse, growth, and rod internal pressure were calculated for DXD4 and Zircaloy-4 clad rods. The DXD4 corrosion and rod growth predictions showed significant improvement over those for Zircaloy-4.

**Table 5.1 Fuel Rod Design Analysis Calculation Results**





**Figure 5.1** Power Histories of the Most-Limiting DXD4 Rods for Corrosion and Rod Internal Pressure Calculations



**Figure 5.2** Power Histories of the Most-Limiting DXD4 Rods for Collapse, AOO Strain, and Steady-State Strain Calculations



**Figure 5.3** Corrosion Predictions for the Most-Limiting Urania and Urania/Gadolinia DXD4 Fuel Rods



**Figure 5.4** Rod Internal Pressure Predictions for the Most-Limiting Urania and Urania/Gadolinia DXD4 Fuel Rods

(This page was intentionally left blank.)

## 6.0 Operational Experience

Siemens has significant experience with the fabrication and irradiation of Duplex cladding. As of April 2000, approximately 580,000 fuel rods with Duplex cladding had been or were under irradiation in fifteen (15) PWRs worldwide, as shown in Table 6.1. The burnup distribution of this fuel is shown in Figure 6.1. A number of different alloys have been used for the outer layer of Duplex cladding; Siemens' experience with Duplex B (DXB) and Duplex D4 (DXD4) cladding is described below.

The largest segment of Siemens' Duplex cladding experience base comes from irradiation of DXB cladding in European PWRs. The inner layer of DXB cladding is Zircaloy-4 with a [

] to provide significant tensile and creep strength to the Duplex cladding. The Alloy B outer layer contains [

]. Table 6.2 lists the plants where DXB has been irradiated since 1992; the burnup distribution of irradiated DXB fuel is shown in Figure 6.2. More than 520,000 fuel rods with DXB cladding have been irradiated in assemblies with arrays ranging from 14x14 to 18x18, reaching an assembly-average burnup of 62 MWd/kgU. Full reload quantities of this cladding have been irradiated and discharged. No problems related to the use of Duplex cladding material in this fuel have been reported, even though some of the fuel has operated in high-temperature plants and under conditions of prolonged nucleate boiling.

The operating experience and burnup distribution of fuel assemblies with DXD4 cladding are shown in Table 6.3 and Figure 6.3, respectively. A small number of fuel rods with DXD4 cladding were first inserted in lead test assemblies in a German PWR in 1989; DXD4 irradiation in the U.S. began with four assemblies in 1994. In-reactor operating experience of DXD4 cladding includes fuel assemblies with rod arrays ranging from 15x15 to 18x18, and extends over five PWRs in which a total of 21,510 rods have been irradiated, up to an assembly-average burnup of 60 MWd/kgU. The highest rod-average burnup reached as of June 2000 is [ ].

Duplex D4 (DXD4) Cladding for PWRs

Because of its superior corrosion resistance, DXD4 cladding is increasingly being used in additional plants to replace both Optimized Zircaloy-4 and DXB claddings. Full reloads of fuel with DXD4 cladding are currently being fabricated, including twenty MOX assemblies that are in their first cycle of operation and twenty MOX assemblies scheduled for delivery in early 2001 to a PWR in Switzerland. Table 6.4 lists the range of fuel rod diameters and fuel pellet stack lengths, core inlet and outlet temperatures, and core average LHGR for the different plants where DXD4 cladding has been used. It should be noted that Plant D24 operates at very high LHGR which typically causes nucleate boiling during two 12-month cycles. Plant B42, a U.S. plant, operates on 18-month cycles.

Siemens' operating experience with Duplex cladding is extensive, and in-reactor performance results are positive. Fabrication of Duplex cladding is routine; ultrasonic testing methods and techniques are fully developed to check bonding of the inner and outer layers, as well as outer-layer thickness uniformity. The process parallels that BWR liner cladding – cladding with nearly two decades of fabrication experience.

**Table 6.1 Operating Experience of Siemens PWR Fuel  
with Duplex Cladding (April 2000)**



**Table 6.2** Operating Experience of Siemens PWR Fuel  
with Duplex B (ELS0.8B) Cladding (April 2000)



**Table 6.3** Operating Experience of Siemens PWR Fuel  
with Duplex D4 Cladding (April 2000)



**Table 6.4** Fuel Rod Parameters and Core Operating Conditions  
for PWRs with DXD4 Fuel Assemblies





**Figure 6.1** Burnup Distribution of Siemens PWR Fuel  
with Duplex Cladding (April 2000)



**Figure 6.2** Burnup Distribution of Siemens PWR Fuel  
with Duplex B (ELSO.8B) Cladding (April 2000)



**Figure 6.3** Burnup Distribution of Siemens PWR Fuel  
with Duplex D4 Cladding (April 2000)

(This page was intentionally left blank.)

## 7.0 Material Properties

### 7.1 *Basic Properties Of Cladding*

#### 7.1.1 As-Manufactured Cladding Properties

Table 7.1 lists the composition and dimensional and mechanical properties of DXD4 cladding manufactured to date by Siemens. Data are provided for each cladding lot of approximately 400 to 800 tubes.

#### 7.1.2 Iodine Stress Corrosion Cracking Behavior

Stress Corrosion Cracking (SCC) results from the accumulation of corrosive iodine and iodine compounds in the pellet- cladding gap, and from a high tangential stress at the cladding inner surface. SCC may occur in the case of a strong pellet- clad mechanical interaction (PCMI). If the local power increases rapidly, fuel thermal expansion deforms the pellets. The fuel pellets impose their deformation on the cladding, which deforms elastically. For sufficiently fast increases in power, the hoop stress in the cladding at high power depends only on the imposed hoop elastic strain and Young's modulus. If the deformation is maintained, the stresses relax at a rate determined by the creep properties of the fuel and cladding. Fuel gaseous swelling can also affect stress relaxation.

Because the inner layer of DXD4 cladding is made of Zircaloy-4, the Young's modulus at the cladding inner surface is the same as that of through-wall Zircaloy-4 cladding. Thus, the maximum hoop stress at the cladding inner surface during a power increase is the same for DXD4 and through-wall Zircaloy-4 claddings when subjected to the same deformation. If the high power level is maintained, the hoop creep rate and hoop stress relaxation rate at the cladding inner surface depend essentially on the local creep properties of the cladding material, i.e., Zircaloy-4. The susceptibility of DXD4 cladding to SCC is therefore similar that of through-wall Zircaloy-4 cladding.

### 7.2 *Correlations and Model Parameters Used for Fuel Performance Analysis*

#### 7.2.1 Density

Zircaloy density is not used in the RODEX2 fuel performance code (Reference 5); it is used only to determine the fuel assembly weight in seismic analyses. Small variations of the tin,

iron, and nickel contents between SPC's through-wall Zircaloy-4 cladding and DXD4 cladding do not significantly affect the crystal lattice parameters and hence the density of Zircaloy in the alpha phase. Furthermore, because the D4 material in the DXD4 cladding tubes accounts for only a fraction [ ] of the cladding weight, which in turn is only a fraction of the total assembly weight, the Zircaloy-4 density used in seismic analyses is also used for DXD4 cladding.

### 7.2.2 Thermal Expansion

The RODEX2 fuel performance code uses the thermal expansion correlation of Kearns (Reference 9). This correlation compares well with the MATPRO model (Reference 10) to predict the circumferential thermal expansion of Zircaloy-4 cladding with typical values of the texture coefficients (Kearns factors). Small variations of the tin, iron, and nickel contents between Zircaloy-4 and the D4 alloy do not significantly affect the crystal lattice parameters and hence the density of Zircaloy at any temperature in the alpha phase. Thermal expansion, the change in density with temperature, is therefore similar for both materials. [ ]

### 7.2.3 Thermal Conductivity

RODEX2 uses a thermal conductivity correlation derived from experimental data obtained by Scott (Reference 11). This correlation is consistent with the MATPRO correlation (Reference 10), which is valid for both Zircaloy-2 and Zircaloy-4.

The thermal conductivity of Zircaloy is primarily a function of temperature. Other characteristics such as residual stress levels, crystal orientation, and minor composition differences [ ], have only a secondary influence on thermal conductivity (Reference 10, pp. 4-16).

The alloy chemistry and heat transfer properties of Zircaloy-2 and Zircaloy-4 with various textures are similar enough that they are considered to be valid for both materials. The

differences in thermal conductivity between the materials appear to be of the same magnitude as the statistical scatter in the data (Reference 10, pp. 4-18).

Because Zircaloy-4 makes up [

], the RODEX2 thermal conductivity correlation is applicable to DXD4 cladding.

#### 7.2.4 Young's Modulus and Poisson's Ratio

Young's modulus and Poisson's ratio are affected primarily by temperature and oxygen content of the alloy; fast fluence, cold work, and texture effects are not as important (Reference 10, pp. 4-41 and 4-46). Small variations in the tin, iron, and nickel contents do not significantly affect the elastic properties of the cladding in the alpha phase. In the MATPRO library (Reference 10), a unique Young's modulus correlation is recommended, whatever the zircaloy composition. Young's modulus and Poisson's ratio for the D4 alloy are consequently only slightly different from those of SPC's standard Zircaloy-4. Because Zircaloy-4 makes up [

], this small change does not significantly affect the elastic behavior of the cladding. Therefore, the Young's modulus correlation (Reference 12) used in RODEX2 for Zircaloy-4 and the RODEX2 value for Poisson's ratio are also applicable to DXD4 cladding.

#### 7.2.5 Thermal and Irradiation-Induced Creep

Creep of DXD4 cladding is discussed in Section 4.1.2 and Appendix A. The thermal creep of the D4 material is faster than that of cold-worked, stress-relieved Zircaloy-4. This contributes to increase the total (thermal + irradiation-induced) circumferential creep strain of DXD4 cladding compared to Zircaloy-4.

In creepdown conditions, the calculated total creep strain of DXD4 cladding is less than [ ] than the calculated creep strain of Zircaloy-4 cladding. This result is confirmed by post-irradiation diameter measurements of DXD4 cladding presented in Table 7.2. Both the observed and calculated creep strain increases, compared to the creep strains of Zircaloy-4 cladding, are within the variability of the permanent circumferential strain.

The overall cladding creep properties used in the calculations for DXD4 cladding are essentially the same as those approved for Zircaloy-4 in RODEX2 (Reference 5).

#### 7.2.6 Irradiation-Induced Growth

The maximum and minimum growth correlations developed in Section 4.1.7 are used for axial growth design calculations. For the RODEX2 fuel performance code (Reference 5), the nominal previously approved growth for Zircaloy-4 is retained for the code pressure, temperature, and strain calculations. This RODEX2 equation is very close to the nominal growth determined for DXD4 and has also been retained in the RODEX2 strain verification for DXD4.

#### 7.2.7 Fatigue Design Curve

Cyclic mechanical strains can cause cumulative damage and subsequent failure which may be predicted by fatigue analysis techniques. O'Donnell and Langer (Reference 6) have developed a Zircaloy fatigue analysis design curve based on fatigue tests with a safety a factor of 2 on stress amplitude or a factor of 20 on number of cycles, whichever is the most limiting. This curve is used for both SPC's standard Zircaloy-4 and DXD4 claddings.

### 7.3 ***LOCA-Related Properties: Specific Heat and Enthalpy***

Small variations in the tin, iron, and nickel contents of zircaloy are expected to have only small effects on the specific heat of the material in either the alpha or beta phases. The transition temperature in the D4 material might be somewhat different from that of Zircaloy-4, but because the phase change enthalpy increase is distributed over a 170 K temperature range, a small change of the transition temperature would not significantly affect cladding temperature predictions. In MATPRO (Reference 10), the specific heats of Zircaloy-2 and Zircaloy-4 are similar enough to consider them to be a single material.

Because the D4 material makes up [ ], and because the cladding transient temperature is controlled mainly by the specific heat of the fuel, the zircaloy specific heat correlations used in SPC's LOCA models to calculate the cladding temperature are applicable to DXD4 cladding.

**Table 7.1 Characteristics of Manufactured DXD4 Cladding Lots**



**Table 7.1** Characteristics of Manufactured DXD4 Cladding Lots *(continued)*



**Table 7.1** Characteristics of Manufactured DXD4 Cladding Lots *(continued)*



**Table 7.1** Characteristics of Manufactured DXD4 Cladding Lots *(continued)*



**Table 7.2 Measured and Calculated Creepdown  
Permanent Strains for DXD4 Clad Fuel Rods**



(This page was intentionally left blank.)

## 8.0 References

1. EMF-92-116(P)(A) Revision 0, *Generic Mechanical Design Criteria for PWR Fuel Designs*, Siemens Power Corporation, February 1999.
2. NUREG-0800, *Standard Review Plan for the Review of Safety Analysis Reports for Nuclear Power Plants*, U.S. Nuclear Regulatory Commission, (1st Edition) November 1975, (2nd Edition) March 1980, (3rd Edition) July 1981.
3. ASME Boiler and Pressure Vessel Code, Section III, Division 1, Article III-2000, *Design Stress Intensity Values for Class 1 Components*, 1977.
4. R. J. Roark, *Formulas for Stress and Strain*, 4th Edition, Table VIII, p. 172.
5. XN-NF-81-58(P)(A) Revision 2 and Supplements 1 and 2, *RODEX2 Fuel Rod Thermal-Mechanical Response Evaluation Model*, Advanced Nuclear Fuels Corporation, June 1990.
6. W. J. O'Donnell and B. F. Langer, "Fatigue Design Bases for Zircaloy Components", *Nuclear Science and Engineering*, Volume 20, January 1964.
7. XN-NF-82-06(P)(A) Revision 1 and Supplements 2, 4, and 5, *Qualification of Exxon Nuclear Fuel for Extended Burnup*, Exxon Nuclear Fuel Company, October 1986.
8. EMF-93-074(P)(A) Revision 0 and Supplement 1, *Generic Mechanical Licensing Report for Advanced 17x17 Fuel Design*, Siemens Power Corporation, June 1994.
9. J. J. Kearns, *Thermal Expansion and Preferred Orientation in Zircaloy*, WAPD-TM-472, November 1965.
10. NUREG/CR-6150, EGG-2720, Volume IV, *SCDAP/RELAP5/MOD3.1 Code Manual, Volume IV: MATPRO – A Library of Materials Properties for Light-Water-Reactor Accident Analysis*, U.S. Nuclear Regulatory Commission, November 1993.
11. D. B. Scott, *Physical and Mechanical Properties of Zircaloy-2 and -4*, WCAP-3269-41, May 1965.
12. E. Duncombe, *Analysis of Void Migration, Clad Collapse and Fuel Cracking in Bulk Oxide Fuel Rods*, WAPD-TM-794, July 1968.

Duplex D4 (DXD4) Cladding for PWRs

---

(This page was intentionally left blank.)

## Appendix A Thermal Creep of DXD4 Cladding

The thermal creep deformation of the DXD4 cladding two-layered cylindrical shell structure, with different creep strengths for the two layers, can be analyzed using a simple theoretical model. This model uses the thin-wall approximation and the compatibility requirement for the strain and strain rate of the two adjacent layers. It also uses the force equilibrium condition in the circumferential direction. A power law is used to describe the creep strain rate.

According to the geometric constraint of the strain compatibility requirement, the creep strain rate of the base layer, denoted by subscript 1, and that of the outer layer, denoted by subscript 2, must be equal to each other and to the overall creep strain rate of the composite structure:

$$\frac{d\varepsilon}{dt} = K\sigma^n = K_1\sigma_1^n = K_2\sigma_2^n \quad (\text{A.1})$$

In Equation A.1, the stresses  $\sigma_1$  and  $\sigma_2$  acting in the circumferential direction upon the two layers are linked by the following force equilibrium equation:

$$f_1\sigma_1 + f_2\sigma_2 = \sigma \quad (\text{A.2})$$

where  $\sigma$  is the total circumferential stress acting upon the cladding, and  $f_1$  and  $f_2$  are the fractional wall thickness of the two layers, which sum to unity. Equation A.1 can be used to calculate the two layer stresses as function of the total stress. After introducing these values into Equation A.2, the equivalent creep factor,  $K$ , can be expressed as:

$$K = \frac{1}{\left(\frac{f_1}{K_1^{1/n}} + \frac{f_2}{K_2^{1/n}}\right)^n} \quad (\text{A.3})$$

$K$  in Equation A.3 reduces to  $K_1$  if  $f_2$  is equal to zero (and, correspondingly,  $f_1$  is equal to unity), which is the case for through-wall cladding, which has no outer D4 layer. The ratio of the equivalent creep factor,  $K$ , to that of the base layer,  $K_1$ , can be expressed in terms of the ratio,  $\rho$ , of the creep factors of the outer layer and the base layer, i.e.,  $\rho = K_2/K_1$ . If

the outer layer is deforming by creep more than the inner layer, then  $\rho$  is greater than unity. The following expression for K in terms of  $\rho$  can be derived from Equation A.3:

$$\frac{K}{K_1} = \frac{1}{\left(f_1 + \frac{f_2}{\rho^{1/n}}\right)^n} \quad (\text{A.4})$$

In tests (Reference A.1) performed on a material with a chemical composition similar to that of the D4 material used for DXD4 cladding, values of  $\rho$  in the range 24 to 95 were determined. These  $\rho$  values result in an expected increase in creep strain rate by a factor between 1.20 and 1.84 for a D4 layer fractional thickness in the range 0.11 to 0.136, similar to the fractional thickness of the D4 layer in the DXD4 cladding of the 18x18 lead fuel assemblies built for the German Convoy-type reactors. Creep tests on DXD4 cladding (Table A.1 below) run for up to 240 hours at 382°C and 120 MPa showed values for  $K/K_1$  in the range 1.15 to 1.30. These results agree well with the lower end of the theoretically determined  $\rho$  domain.

[

] Moreover, comparison of creep test results (see Table A.1 below) for low-tin Zircaloy-4 cladding and DXD4 cladding (with an outer-layer fractional thickness of [     ]) showed that the DXD4 cladding thermal creep strain rate was within the scatter band of the thermal creep strain rate of the Zircaloy-4 cladding.

The total creep strain of the cladding is the sum of the thermal creep strain and of the irradiation-induced creep strain, which is presumed to be the same for the D4 outer layer as for the standard Zircaloy-4 material of the base layer. While the thermal creep strain rate is monotonically decreasing (as the inverse of the square root of time for constant

temperature and stress), the irradiation creep strain is continuously increasing with burnup. Soon after the start of irradiation, the irradiation creep component becomes dominant, and by the end of the irradiation life, the thermal creep strain contributes only  $1/9$  to  $1/10$  of the total creep strain. Under these conditions, even considering the maximum thermal creep enhancement of [ ] outer-layer fractional thickness (determined above), the impact on the total creep strain would be an increase on the order [ ], which is minimal and well within the variability of the total strain of the through-wall Zircaloy-4 cladding.

**Table A.1** Creep Strain (%) During Biaxial Creep Tests at 382°C and 120 MPa Circumferential Stress for DXD4 and Zircaloy-4 Claddings



**References**

- A.1 E. R. Bradley and A. L. Nystrom, "Microstructure and Properties of Corrosion-Resistant Zirconium-Tin-Iron-Chromium-Nickel Alloys," *Proceedings of the Tenth International Symposium on Zirconium in the Nuclear Industry, ASTM STP 1245*, American Society for Testing and Materials, 1993.

## Appendix B Corrosion Behavior of DXD4 Cladding

### Summary

Alloy D4, the outer layer of DXD4 cladding, has greatly improved waterside corrosion behavior compared to both standard Zircaloy-4 and Optimized Zircaloy-4 (low-tin Zircaloy-4 as specified by Siemens). Siemens has measured the post-irradiation oxide thickness of DXD4 cladding in five PWRs. Data include measurements made after multiple, consecutive reactor cycles in a high-temperature plant, up to a rod-average burnup of approximately [ ] MWd/kgU; the highest oxide thickness measured at this burnup was [ ] microns.

Measured oxide thickness data, along with power history information and other relevant reactor operating data, have been used to develop and benchmark a modified corrosion model that is incorporated in SPC's fuel performance code. Observations and oxide thickness measurements indicate that the rate of corrosion of DXD4 cladding increases when the thickness of the oxide layer reaches approximately [ ] microns. The modified corrosion model incorporates a "second-transition" model to account for the increased corrosion rate that may occur at high burnup. The corrosion subroutine in SPC's fuel performance code that incorporates the second-transition model is called CORROS II. It is shown that CORROS II accurately predicts the peak oxide thickness of fuel rods as a function of burnup up to burnups as high as [ ] MWd/kgU.

### B.1. *Oxidation*

Fuel with DXD4 cladding has been irradiated in five PWRs: one in the U.S., one in Switzerland, and three in Germany. Core operating conditions for these plants are listed in Table B.1. As shown in the table, Plant D24 operates at very high average power and at a high coolant exit temperature. Post-irradiation poolside oxide thickness measurements made at each of the five plants form the basis for the development and benchmarking of SPC's corrosion model, CORROS II, for DXD4 cladding.

Siemens has used two different techniques to measure oxide thickness. In the first (and more common) technique, the oxide thickness was measured along the length of the fuel rod, either along a helical path or along a straight-line path. In cases where, for ease of

measuring, the fuel rods were not removed from the assembly, data were obtained only for peripheral fuel rods, in the spans between the spacers.

Data collected using the first measurement technique are listed in Table B.2. The table shows the plant designation (SPC PWR code) where the data were taken, fuel assembly number, fuel rod location, fuel rod burnup and cycles of irradiation, and the measured maximum oxide thickness. The maximum oxide thickness is defined as the highest mean value of measurements averaged over a running length of 40 mm moving along the rod. This differs from SPC's measurement reporting for Zircaloy-4, which used the local peak of the linear trace.

In the second technique, oxide thickness measurements were made at a single elevation within an assembly. Data for all of the rods were obtained at the mid-span elevation of the span where the highest oxide thickness was expected, by moving a slender wand with two oxide probes at its tip in and out between the rows of fuel rods. As the probes passed through the assembly, and at a discrete point on each fuel rod, data were collected for all rods on both sides of a row during both insertion and withdrawal. In the fuel exam where this technique was used, all rows of two adjacent sides of the assembly were measured. The reported data are the average of the measurements (typically four to eight per fuel rod) for each fuel rod.

Data collected using the second technique, used at Plant B42, are given in Table B.3. For purposes of plotting and for some of the calculations, this overall data set was further reduced by dividing the set of 264 data points (representing 264 fuel rods) into 11 groups of between 20 and 27 data points, each group defining a relatively narrow burnup range. Table B.4 lists the burnup range, number of data points, and the average and standard deviation of rod oxide thicknesses in each burnup group.

The data from Tables B.2 and B.4 are plotted in Figure B.1 as measured maximum oxide thickness as a function of fuel rod average burnup. Measurement uncertainty for the oxide thickness measurement techniques used by Siemens is typically about four microns. Because the techniques are based on the measurement of probe liftoff from the unoxidized cladding surface, measurements are easily affected by crud on the fuel rods and can

therefore be biased high. This bias disproportionately affects measurements of thin oxide layers. For this reason, data obtained at rod burnups [ ] were omitted from further evaluation.

SPC has used one additional set of data for determining parameter values for the second-transition model subroutine. These data consist of helical oxide thickness scans along the full fuel rod length. The data, shown in Figures B.2 through B.6, show the oxide thickness at every point along the fuel rods. Figures B.2 through B.4 show oxide thickness data during consecutive cycles, up to five cycles of irradiation. The acceleration of oxide thickness growth in the upper part of the fuel rods during later cycles, when the rods reached high burnups, is apparent in these plots.

Representative power histories of fuel rods irradiated at Plants D24 and D18 are shown in Figure B.7. Note the very high LHGR throughout rod exposure for the rods irradiated at Plant D24.

## B.2. *Corrosion Model*

SPC has modified the MATPRO-based corrosion model, CORROS, to describe the oxide thickness growth of DXD4 cladding. The modified corrosion model, CORROS II, takes into account the acceleration of oxide growth, here termed the second transition, which may be observed at high burnup. Three corrosion regimes (pre-transition, post-transition/pre-second-transition, and post-second-transition) are therefore considered and the following correlations based on the MATPRO corrosion model apply:



The corrosion parameter (E), the increase in corrosion rate (I) after the second transition, and the oxide thickness ( $x^{ST}$ ) at which the second transition occurs have been determined for DXD4 cladding using statistical methodology and regression analysis. A 95/95 upper-bound multiplier has also been determined by these analyses.

Oxide thickness measurement data from three reactors (Plants D18, D21, and D24) were used to derive CORROS II model parameters E, I, and  $x^{ST}$ . Model predictions were then

compared with measured oxide data from the five PWRs where oxide thickness measurements were made. Each of the data points in the data set used to determine E, I, and  $x^{ST}$  represents the highest measured oxide thickness of a single fuel rod. Some of the rods were measured in consecutive cycles. As explained in Section B.1 above, a small number of data points from measurements of low-burnup, low-oxide-thickness Plant D18 fuel rods were omitted from consideration.

### B.2.1 Corrosion Parameter E

The reactor core inlet temperature, thermal-hydraulic conditions, fuel rod power histories, and fuel rod axial power shape are used as input to SPC's fuel performance code to calculate the cladding metal-to-oxide interface temperature at each step of the oxide thickness calculation. The effect of the growing oxide film on the metal-to-oxide interface temperature is taken into consideration. A thermal conductivity of [

B.1 ] is assumed for heat transfer through the oxide layer.

For each of the DXD4 cladding corrosion data points, a value of E was determined such that the calculated oxide thickness matched the measured oxide thickness. Statistical methodology and regression analyses, as previously described in Reference B.2, were then used to determine the best estimate of E and I for all of the DXD4 data. The regression analysis has the format:

$$\frac{\text{Measured Oxide Thickness}}{\text{Calculated Oxide Thickness}} = C$$

where C is the regression constant. The best-fit condition occurs when C is unity. For oxide thicknesses of [ ], the best fit of the DXD4 cladding corrosion data was obtained when the value of E was [ ].

### B.2.2 Second-Transition Corrosion Model

Measured oxide thickness data from Plant D24 are compared in Figure B.8 to values predicted by the MATPRO corrosion model without the second transition. The measured data show a late-in-life increase in corrosion rate, and hence data at approximately [ ] MWd/kgU burnup are slightly underpredicted by the unmodified MATPRO model, and data

at approximately [ ] MWd/kgU are significantly underpredicted. Inspection of Figures B.2 through B.6 shows that enhanced corrosion commences first in the upper part of the fuel rods, where the oxide layer thickness is approximately [ ] microns. The lower part of the rods, where the burnup and fluence are nearly identical to that in the upper part of the rods, does not show this acceleration in oxide growth. The second transition in corrosion rate, therefore, appears not to be dependent on burnup or fluence, but occurs when the oxide thickness has reached approximately [ ] microns. Regression analyses of the high-burnup data from Plant D24 and the data shown in Figures B.2 through B.6 showed that, for DXD4 cladding, the corrosion rate after this transition at [ ] microns is [ ] times the rate before the transition.

### B.2.3 Upper-Bound Multiplier

Oxide thickness calculations for all rods from Plants D18, D21, and D24 were repeated with a corrosion parameter of [

]. Using the methodology described in Reference B.2, the standard deviation of the calculated values was derived and expressed as a fraction or percentage.

Based on a method described by Owen (Reference B.3), the 95/95 upper-bound value for calculated oxide thickness can be determined by multiplying the best-estimate value by a 95/95 upper-bound multiplier derived from the calculated standard deviation. The value of this multiplier was determined to be [ ].

## B.3. *Corrosion Model Verification*

CORROS II model predictions have been verified against oxide thickness data obtained from measurements at five PWRs. The second-transition model was verified separately against full-length rod scans at two of the plants.

### B.3.1 Best Estimate and 95/95 Upper Bound

Figure B.9 shows a comparison of measured peak oxide thickness from Plants D18, D21, and D24, and oxide thickness calculated using the CORROS II model, with [

]. The best-estimate and 95/95 upper-bound values are indicated in the figure. Except for some of the measurements at low burnup, which, as explained earlier, are biased high due to measurement technique limitations, all of the data fall within the calculated 95/95 upper bound.

The calculated oxide thickness for rods at Plants D18 and D24 is plotted as a function of burnup in Figures B.10 and B.11. The best-estimate maximum oxide thickness and 95/95 upper bound for these data were calculated using a single Plant D18 fuel rod power history for the Plant D18 predictions, and a single Plant D24 rod power history for the Plant D24 predictions. Figures B.10 and B.11 show that agreement between the measured maximum oxide thickness and the calculated oxide thickness is very good over the entire burnup range. The acceleration in the corrosion rate (at burnups above approximately [ ] MWd/kgU) is predicted with good accuracy.

CORROS II and the corrosion parameters established for DXD4 cladding were further used to compare the calculated and measured data, listed in Tables B.2 and B.3, respectively, from Plants D14 and B42. The power history applicable to each fuel rod (or group of rods for Plant B42) was used in calculating the expected maximum oxide thickness. The results of these calculations are shown in Figure B.12, where the calculated oxide thickness is compared to the measured oxide thickness. The calculated 95/95 upper bound is also shown. It is noted that most of the data are slightly overestimated. This is attributed to the effects of intermediate flow mixers in the upper spans of the Plant D18 and Plant B42 fuel assemblies. The mixers provide extra cooling of the cladding in the upper spans of the assembly; this extra cooling is not modeled by SPC's fuel performance code. Thus, the cladding temperature calculated by the code is higher than the actual metal-to-oxide interface temperature in the spans with maximum oxide thickness, leading to a slight overestimation of the peak oxide thickness for rods in PWR assemblies with intermediate flow mixers.

### B.3.2 Accelerated Corrosion

To further verify that CORROS II accurately predicts the observed acceleration in corrosion rate at an oxide thickness of approximately [ ] microns, SPC performed additional

calculations. The oxide thickness along the length of several fuel rods from Plants D18 and D24 is compared with CORROS II predictions in Figures B.13 through B.17. These calculations model the metal-to-oxide interface temperature along the full rod length and use the corrosion factors established for DXD4 cladding, as previously described. The predictions closely match the measured data through successive cycles of irradiation, including the accelerated growth that occurs late in life in the upper part of the fuel rods. This indicates that the second-transition acceleration in corrosion rate is accurately modeled by CORROS II.

#### B.4. **Conclusions**

The CORROS II corrosion model has been developed to predict the corrosion behavior of zirconium-alloy cladding up to burnups of approximately [ ] MWd/kgU. The model includes a second-transition subroutine that models the increase in oxide growth rate which may occur late in life. Statistical methodology and regression analyses were used to determine the value of four separate parameters in the CORROS II methodology. The corrosion behavior of DXD4 cladding is accurately predicted, up to a burnup as high as [ ] MWd/kgU, with the following parameters:

[

]

#### B.5. **References**

- B.1 E. R. Bradley and A. L. Nystrom, "Microstructure and Properties of Corrosion-Resistant Zirconium-Tin-Iron-Chromium-Nickel Alloys," *Proceedings of the Tenth International Symposium on Zirconium in the Nuclear Industry, ASTM STP 1245*, American Society for Testing and Materials, 1993.
- B.2 ANF-88-133(P)(A), *Qualification of Advanced Nuclear Fuels PWR Design Methodology for Rod Burnups of 62 GWd/MTU*, Advanced Nuclear Fuels Corporation, December 1991.
- B.3 D. B. Owen, "Factors for One-Sided Tolerance Limits and for Variables Sampling Plans," U.S. Department of Commerce, March 1963.

**Table B.1 Operating Conditions of PWRs Where  
DXD4 Cladding Corrosion Was Measured**



**Table B.2 DXD4 Fuel Rod Maximum Oxide Thickness, Line-Contact Method**



**Table B.3 DXD4 Fuel Rod Maximum Oxide Thickness, Point-Contact Method**



**Table B.3** DXD4 Fuel Rod Maximum Oxide Thickness, Point-Contact Method *(continued)*



**Table B.3** DXD4 Fuel Rod Maximum Oxide Thickness, Point-Contact Method *(continued)*



**Table B.3** DXD4 Fuel Rod Maximum Oxide Thickness, Point-Contact Method *(continued)*



**Table B.4** Maximum Oxide Thickness of DXD4 Fuel Rods  
Irradiated at Plant B42





**Figure B.1** DXD4 Cladding Oxide Thickness as a Function of Burnup



**Figure B.2** Measured Axial Oxide Profile for Plant D24, Assembly 16-01, Rod L05 through Successive Cycles of Irradiation



**Figure B.3** Measured Axial Oxide Profile for Plant D24, Assembly 16-01, Rod L02 through Successive Cycles of Irradiation



**Figure B.4** Measured Axial Oxide Profile for Plant D24, Assembly 16-01, Rod L01 through Successive Cycles of Irradiation



**Figure B.5 Measured Axial Oxide Profile for Plant D18, Assembly 0366, Rod N14  
after Four Cycles of Irradiation**



**Figure B.6 Measured Axial Oxide Profile for Plant D18, Assembly 0366, Rod R13  
after Four Cycles of Irradiation**

**Figure B.7** Typical Fuel Rod Power Histories for Plants D18 and D24

**Figure B.8** DXD4 Cladding Oxide Predictions for Plant D24 without the Second-Transition Model Compared to Measured Data, Indicating Underprediction at High Burnup



**Figure B.9** Comparison of Measured and CORROS II-Calculated Oxide  
for Plants D18, D21, and D24



**Figure B.10** Comparison of Measured Oxide Thickness and Predicted Best-Estimate and 95/95 Upper-Bound Corrosion of Plant D18 Fuel Rods



**Figure B.11** Comparison of Measured Oxide Thickness and Predicted Best-Estimate and 95/95 Upper-Bound Corrosion of Plant D24 Fuel Rods



**Figure B.12** Comparison of Measured and CORROS II-Calculated Oxide  
for Plants B42 and D14



**Figure B.13** Measured Axial Oxide Profile and CORROS II-Calculated Data for Plant D24,  
Assembly 16-01, Rod L05 through Successive Cycles of Irradiation



**Figure B.14** Measured Axial Oxide Profile and CORROS II-Calculated Data for Plant D24,  
Assembly 16-01, Rod L02 through Successive Cycles of Irradiation



**Figure B.15** Measured Axial Oxide Profile and CORROS II-Calculated Data for Plant D24, Assembly 16-01, Rod L01 through Successive Cycles of Irradiation



**Figure B.16** Measured Axial Oxide Profile and CORROS II-Calculated Data for Plant D18, Assembly 0366, Rod N14 after Four Cycles of Irradiation



**Figure B.17** Measured Axial Oxide Profile and CORROS II-Calculated Data for Plant D18, Assembly O366, Rod R13 after Four Cycles of Irradiation

## Appendix C Hydrogen Pick-up and Hydride Distribution

### Summary

Samples from five DXD4 clad fuel rods irradiated for up to four cycles (up to 55.6 MWd/kgU burnup) in one PWR were measured for oxide thickness, hydrogen content, and hydrogen pick-up. Hydrogen pick-up fraction was determined for each cladding sample. Metallographic cross-sections were prepared, and the hydride distributions and orientations after irradiation and oxidation were analyzed. The hydrogen pick-up fraction of DXD4 cladding at the oxide thickness level at which measurements were made is [ ]. A conservative estimate indicates that for 17x17-type cladding up to a burnup of [ ] MWd/kgU (equivalent to [ ] microns of oxide), a hydrogen concentration of [ ] ppm or less is expected. As in Zircaloy-4 cladding, zirconium hydrides accumulated near the cooler outer surface of the DXD4 cladding; DXD4 cladding's D4 alloy outer layer did not appear to have a strong influence on the distribution of hydrides. The hydrides in DXD4 cladding precipitated mainly in the tangential direction; radially precipitated hydrides were largely absent.

### C.1. *Introduction*

In the corrosion reaction of water with zirconium-alloy clad fuel rods, hydrogen is formed through the decomposition of water. Part of the hydrogen is released into the coolant and another part enters the cladding. The hydrogen that is taken up by the cladding remains initially in solid solution. When the level of hydrogen reaches a critical concentration, zirconium hydrides precipitate. Hydrogen solubility in zirconium-based alloys is weakly dependent on alloy composition and metallurgical structure, and more strongly dependent on temperature, solubility being lower at lower temperatures. At room temperature, the solubility of hydrogen in zirconium-based alloys is less than a few parts per million (ppm).

Due to the temperature gradient in the cladding during fuel rod operation, zirconium hydrides have a tendency to precipitate near the outer surface of the cladding, where the temperature, and hence the hydrogen solubility, is lowest. At 300°C, the mean hydrogen solubility of zircaloy-type alloys is around 70 ppm. Because high levels of hydrides may adversely affect the mechanical properties of zirconium alloys, especially near room

temperature, SPC has determined the amount of hydrogen picked up by DXD4 cladding during irradiation. Metallographic cross-sections of the cladding after irradiation were evaluated to determine the distribution and orientation of the zirconium hydrides.

### C.2. *Experimental Results*

Cladding hydrogen concentration of four fuel rods with DXD4 cladding irradiated at PWR D18 was determined at the hot cells of the TransUranium Institute (ITU) in Karlsruhe, Germany. The rods had been irradiated for three and four cycles, up to a burnup of 55.6 MWd/kgU. Each rod typically was analyzed at the location of thickest oxide; one rod was analyzed at two locations. Three to five samples were used in the hot gas extraction technique for determination of each data point. In each case, samples were analyzed with the oxide still attached. The data thus obtained are listed in Table C.1. The average pick-up fraction for the data reported in Table C.1 is [      ]. Metallographic samples were taken adjacent to the samples for hydrogen extraction analysis. After appropriate etching, the hydrogen distribution and orientation of the hydrides was determined from the metallographic cross-sections.

**Table C.1** Hydrogen Pick-up Data for DXD4 Cladding at PWR D18

In the data reported here, it was assumed that all of the hydrogen extracted came from the metal part of the samples and that the adherent oxide was free of hydrogen or hydrogen-containing species. It has recently been shown (Reference C.1) that this assumption leads

to an overestimate, from 5 to 20%, of the amount of hydrogen in the metal. In Reference C.1, the oxide was shown to contain, on average, approximately 1000 ppm of hydrogen, regardless of the amount of hydrogen in the metal and independent of the oxide thickness.

### C.3. *Discussion*

The hydrogen pick-up fraction of DXD4 cladding is shown as a function of local fuel rod oxide thickness, along with similar data for Zircaloy-4 cladding, in Figure C.1. The pick-up fraction of DXD4 cladding was calculated with the following relation:



The correlation contains a correction factor to account for the fraction of metal mass of the overall sample weight due to the weight of the adherent oxide. The oxide is assumed to be 100% dense. There is no correction to account for partitioning of hydrogen between the metal and the adherent zirconium oxide. The actual hydrogen concentration in the metal is, therefore, estimated to be approximately 8% less than the values reported in Table C.1 if it is assumed that the adherent oxide contained 1000 ppm hydrogen (Reference C.1).

Inspection of the Zircaloy-4 data shown in Figure C.1 reveals that the hydrogen pick-up fraction diminishes with increasing oxide thickness. This is assumed to be due to the

oxide layer forming a more protective barrier to hydrogen penetration as the layer gets thicker. One DXD4 cladding data point at [ ] of oxide thickness appears to lie outside the range of the other data. Such outlying data have also been observed for Zircaloy-4 cladding, as shown in Figure C.1. It is noted that a small change in oxide thickness measurement can lead to a fairly significant change in calculated hydrogen pick-up fraction. The outlying value may, therefore, be due to uncertainties in the measurement of oxide thickness or the determination of hydrogen content.

Hydrogen concentration for DXD4 cladding is shown as a function of oxide thickness in Figure C.2. In this figure, a constant hydrogen pick-up fraction is represented by a straight line. Figure B.11 indicates that at a burnup of [ ] MWd/kgU, the maximum oxide thickness at the 95/95 level in Plant D24 is [ ] microns. Linear extrapolation of the data at a constant pick-up fraction indicates that at an oxide thickness of [ ] microns, the expected hydrogen level in DXD4 cladding would be [ ] ppm. This amounts to a hydrogen pick-up fraction of approximately [ ] for 17x17 PWR design cladding. As stated earlier, the average pick-up fraction for the data reported in Table C.1 is [ ]. Considering the diminishment of hydrogen pick-up with increasing oxide thickness, and the assumption that all of the hydrogen detected in the hot extraction analyses was contained in the metal – whereas a significant portion of the hydrogen actually comes from the oxide (see Reference C.1), the extrapolation is conservative for cladding with thicker oxide, as indicated in Figure C.1. SPC therefore expects that, for DXD4 cladding up to an exposure of [ ] MWd/kgU, a hydrogen concentration of [ ] ppm in the metal will normally not be exceeded. This level of hydrogen has been shown to have negligible impact on cladding ductility beyond the reduction in ductility due to neutron irradiation at intermediate to high burnups.

#### C.4. *Metallographic Observations*

Metallographic cross-sections of DXD4 cladding showing the hydride distribution and orientation after irradiation and oxidation are shown in Figures C.3 through C.5. For comparison, cross-sections of through-wall Zircaloy-4 cladding are shown in Figures C.6 and C.7.

Figure C.3 shows a cross-section of Rod A09 (see Table C.1). At the location shown – the location of the rod’s highest oxide thickness – the cladding contains [ ] ppm of hydrogen. The concentration of hydrides, all of which are oriented in the tangential direction, is somewhat higher near the cladding outer surface. During reactor operation, only about [ ] ppm of the hydrogen in the cladding was in the form of hydrides that had precipitated; the remaining [ ] ppm of hydrogen remained in solution. Many of the hydrides visible in the micrograph, therefore, precipitated during cooldown of the cladding after reactor shutdown.

The hydride distribution in a sample from Rod G01, with [ ] ppm of hydrogen and [ ] microns of oxide, is shown in Figure C.4. The concentration of hydrides near the cladding outer surface is clearly higher than in the remainder of the sample. In addition to hydrides near the cladding outer surface, some hydrides have preferentially precipitated at the interface between the cladding’s Zircaloy-4 and D4 layers. It is likely that the hydrides at this interface precipitated during cooldown of the cladding. A wide band of precipitation-free Zircaloy-4 exists adjacent to the interface, and it appears that hydrogen diffused from this region to the interface. The vast majority of hydrides in this sample are oriented in the tangential direction.

Figure C.5 shows a cross-section of a sample from Rod R12, which, at a burnup of 55.6 MWd/kgU, had an oxide layer thickness of [ ] microns and hydrogen content of [ ] ppm, the highest hydrogen level measured in an irradiated DXD4 clad fuel rod. At this hydrogen level, most of the hydrides have precipitated near the cladding outer surface. Although this precipitation of hydrides near the cladding’s outer surface may give the appearance that the hydrides preferentially accumulate in the D4 alloy (the cladding’s outer layer), comparison with Figure C.6, a micrograph of 46.4 MWd/kgU burnup through-wall Zircaloy-4 cladding with [ ] ppm hydrogen and an oxide thickness of [ ] microns, clearly shows that the extent of hydride accumulation near the DXD4 cladding outer surface is about the same as it is in the Zircaloy-4 cladding.

At higher hydrogen concentrations, the hydride precipitation layer near the cladding outer surface becomes quite dense. This behavior is shown in Figure C.7, a micrograph of a

through-wall Zircaloy-4 cladding sample with a burnup of 46.4 MWd/kgU, oxide thickness of [ ] microns, and hydrogen content of [ ] ppm. Overall, therefore, it does not appear that the D4 alloy outer layer has much influence on the precipitation of hydrides, as the greatest accumulation of hydrides in both DXD4 and through-wall Zircaloy-4 cladding occurs near the cladding outer surface. The prevailing temperature gradient, rather than small variations in cladding composition, influences the behavior of hydride precipitation.

Solid zirconium hydride "lenses" in through-wall Zircaloy-4 cladding have been shown to be detrimental to cladding performance during certain accident conditions (RIA, LOCA). These hydride lenses form near the cladding outer surface when small patches of oxide spall off from the cladding surface during operation. Because oxide spalling has never been observed on DXD4 cladding, the formation of hydride lenses has not occurred.

#### C.5. *Conclusions*

The results of hot cell measurements of hydrogen pick-up in DXD4 cladding may be summarized as follows:

- The hydrogen pick-up fraction of DXD4 cladding is approximately [ ]. A conservative linear extrapolation of this value indicates that for 17x17-type cladding up to an exposure of [ ] MWd/kgU, a hydrogen concentration of [ ] ppm will normally not be exceeded.
- Hydrides accumulate in the coldest part of the cladding wall (near the cladding outer surface). DXD4 cladding's D4 alloy outer layer does not appear to have a strong influence on the distribution of zirconium hydrides in irradiated DXD4 cladding.
- The hydrides in DXD4 cladding precipitate mainly in the tangential direction; radially precipitated hydrides are largely absent.

#### C.6. *References*

- C.1 A. Hermann et al., "Hydrogen Distribution Between Fuel Cladding Metal and Overlying Corrosion Layers," *Proceedings of the American Nuclear Society International Topical Meeting on Light Water Reactor Fuel Performance*, April 2000.



**Figure C.1** Hydrogen Pick-up Fraction as a Function of Oxide Thickness



**Figure C.2** Hydrogen Pick-up as a Function of Oxide Thickness



**Figure C.3** Hydride Distribution and Oxide Layer in DXD4 Clad Fuel Rod A09



**Figure C.4** Hydride Distribution and Oxide Layer in DXD4 Clad Fuel Rod G01



**Figure C.5** Hydride Distribution and Oxide Layer in DXD4 Clad Fuel Rod R12



**Figure C.6** Hydride Distribution and Oxide Layer in Zircaloy-4 Clad Fuel Rod V04



**Figure C.7** Hydride Distribution and Oxide Layer in Zircaloy-4 Clad Fuel Rod V04

## Appendix D Stress Rupture and Ballooning Tests

### Summary

Stress rupture and ballooning tests were conducted to compare the behavior of Duplex D4 (DXD4), Duplex B (DXB), and standard through-wall Zircaloy-4 claddings. All cladding used in the tests came from normal production lots; the DXD4 cladding (9.5 mm OD, 8.3 mm ID) came from a production lot that met SPC's specification for DXD4 cladding. DXD4 and DXB cladding differ slightly in the compositions (concentrations of chromium, iron, and tin) of the alloys (Alloy D4 or Alloy B) used for the outer layer, but both types of cladding have a Zircaloy-4 inner layer, and the ratio of the thicknesses of the inner and outer layers is the same.

Over the testing temperature range (700 to 900°C), time to failure in the stress rupture tests for DXD4 cladding was the same or slightly longer for through-wall Zircaloy-4 cladding. The hoop strain at rupture for DXD4 cladding specimens was the same as or lower than for through-wall Zircaloy-4. These results indicate that it is conservative to model DXD4 with the same parameters as used for Zircaloy-4.

### D.1. *Introduction*

Stress rupture and high-temperature ballooning, or cladding swelling, tests are conducted to assess the cladding material behavior during an assumed loss-of-coolant accident (LOCA). The data obtained in the tests provide the experimental basis for the evaluation and calculation of the deformation and rupture of fuel rod cladding under postulated LOCA conditions. The tests described in this appendix were conducted with resistance-heated (ohmic heating) cladding tube sections from standard production lots, under carefully controlled conditions of temperature, temperature distribution (axial and circumferential directions), heating rate, and internal overpressure. Test results for DXD4 cladding were compared to those for Zircaloy-4 cladding and other Duplex cladding to determine whether the methodology developed for zircaloy cladding is applicable to DXD4 cladding.

## D.2. *Test Description*

In the test equipment used for stress rupture and ballooning tests, the cladding sample is held in a vertical position between two fixtures. The lower fixture is free to move in the axial direction of the specimen to accommodate specimen length changes due to thermal expansion, ballooning, and swelling. The upper fixture remains stationary. Both fixtures are connected to an AC power supply which is used to heat the specimen. Specimen temperature is controlled with a programmable control unit connected to thermocouples welded to the test section. A schematic diagram of the test setup is shown in Figure D.1.

The cladding sample is connected to a high-pressure argon gas supply through the upper end cap of the specimen. The initial total gas volume of the test system is approximately 40 cm<sup>3</sup>, of which approximately 4 cm<sup>3</sup> occupies the initial free volume of the specimen and the remainder is maintained as a remote volume kept at 350°C. The gas inventory connected to the specimen remains constant during the test. The ratio of specimen volume to remote volume is such that temperature or volume changes in the specimen have relatively little effect on the internal pressure of the specimen.

A camera measures the outer diameter of the cladding specimen at the rate of three frames per second. The field of view of the camera covers the axial length of the sample where the temperature is measured and where swelling of the specimen is expected. A computer-controlled data acquisition system records temperature, specimen internal overpressure, and camera output for the duration of the test.

## D.3. *Specimen Design*

Each test specimen consists of a 238 mm-long section of cladding fitted with a welded lower end plug. The tube section is filled with annular Al<sub>2</sub>O<sub>3</sub> ceramic pellets, centered by a stainless steel rod, that improve temperature uniformity around the circumference of the specimen. The outer diameter of the pellets is approximately 0.3 mm less than the inner diameter of the cladding tube, except for pellets in the middle of the specimen, where, over a length of 60 mm, pellets with a reduced diameter are used. The reduced-diameter pellets leave a diametral gap between pellets and cladding of 1.3 mm. An expansion gap for the pellets and steel rod is provided at the top of the specimen. An upper end plug,

designed to connect to the pressurization system and remote gas volume, is welded to the upper end of the specimen. The upper and lower ends of the specimen are covered by support sleeves to prevent outward cladding creep and swelling in these regions. The presence of these support sleeves also results in an axial temperature distribution that leads to deformation and rupture within the center section of the specimen, where thermocouples record specimen temperature and a camera records deformation. A schematic diagram of the cladding tube specimen design is shown in Figure D.2.

Figure D.2 also shows the axial and circumferential locations of the Pt-PtRh thermocouples that are spot-welded to the cladding surface. Temperature variations around the circumference of the specimen are measured by three thermocouples at elevation "A." Data from the three thermocouples at elevation "B" are averaged and used for temperature control during the test. The remaining thermocouples are used to determine axial temperature variations.

#### D.4. *Testing Procedure*

In preparation for stress rupture and ballooning tests of a cladding specimen, the outside diameter (OD), inside diameter (ID), and wall thickness variations for the specimen to be tested are measured and recorded. The specimen is then prepared as described in Section D.3 above, fitted with thermocouples, and installed in the test stand. All thermocouples are connected to the programmable control unit and the data acquisition system. The high-pressure argon supply is connected to the specimen and to a digital pressure gauge. Specimens are typically tested in air.

After all connections are checked, the specimen is heated to 350°C. The argon pressure is adjusted to provide the desired initial hoop stress in the cladding, then the argon supply is isolated from both the specimen and the remote-volume flask. The specimen is heated at a controlled heating rate to the predetermined maximum test temperature and held until rupture occurs (stress rupture test), or the specimen may be heated at a controlled rate until it ruptures (transient test).

Typical changes in temperature and pressure as a function of time during these tests are shown in Figure D.3. The temperature is increased from 350°C to the test temperature at

a rate of 50 K/s; the pressure within the specimen remains nearly constant for the duration of the test. Changes in specimen circumferential strain are relatively slow at the start of the test and progress rapidly during the final phase. A typical strain diagram is shown in Figure D.4.

#### D.5. *Comparative Stress Rupture Behavior*

DXD4 specimens were prepared from cladding tubes from a production lot fabricated by NRG (Germany) from a co-extruded tube shell produced by Teledyne Wah Chang (U.S.). The cladding met all specified quality control requirements, including the limits for chemical composition of both the outer-layer D4 alloy and the Zircaloy-4 inner layer. The material certificates are stored in the appropriate archives at Siemens' facilities in Erlangen, Germany.

The through-wall Zircaloy-4 cladding that had been tested previously also came from various cladding lots manufactured by NRG in Germany. Details of the cladding source and properties are given in Table D.1. Both "standard-tin" Zircaloy-4 cladding, with a tin content of approximately 1.5%, and "low-tin" Zircaloy-4 cladding, containing approximately 1.3% tin, have been tested. No discernable difference in the high-temperature stress rupture behavior of these two Zircaloy-4 variants was observed. Both types of cladding have compositions and other attributes that comply with the applicable ASTM specifications.

Results of stress rupture tests performed on low-tin Zircaloy-4 cladding specimens at temperatures between 600 and 900°C are given in Table D.2. All tests were conducted with the specimens at an initial temperature of 350°C. Specimens were heated at a rate of 50 K/s; specimen temperature uniformity was typically within 10 K. For each test, the table lists test specimen designation and cladding lot, nominal test temperature, specimen initial pressure at 350°C, and time to failure.

Time to rupture as a function of initial specimen pressure for low-tin Zircaloy-4 cladding is shown in Figure D.5. The plot shows good agreement between data from different lots of Zircaloy-4 cladding. Time to rupture as a function of initial cladding hoop stress is shown in Figure D.6 for both low-tin and standard-tin Zircaloy-4 cladding. Time to rupture is

plotted as a function of initial hoop stress (rather than pressure) to facilitate the comparison of cladding tubes of different diameters. The measurement results for low-tin cladding compare well with those for higher-tin cladding. Also shown in Figure D.6 are the least-squares fit lines through the data at the different test temperatures. These least-squares correlations are the reference Zircaloy-4 correlations against which the behavior of Duplex cladding was evaluated.

Stress rupture measurements of DXD4 cladding were made in the same manner and with the same equipment used for the Zircaloy-4 measurements. Tests were conducted at temperatures between 700 and 900°C; results are given in Table D.3. Test temperature, specimen initial pressure at 350°C, normalized time to failure (to adjust for off-normal temperature and pressure conditions), and hoop strain at rupture are given. Similar data for DXB cladding are given in Table D.4. The DXB and DXD4 data are shown in Figure D.7 along with the Zircaloy-4 reference curves from Figure D.6. Inspection of Figure D.7 readily reveals that the time to rupture for pressurized tubing specimens ramped to temperatures between 600 and 900°C is essentially the same for Zircaloy-4, DXB, and DXD4 claddings. Figure D.7 further shows that the time to rupture of DXD4 cladding is actually slightly greater than that of through-wall Zircaloy-4 cladding.

#### D.6. *Comparative Ballooning Behavior*

The ballooning, or clad swelling, behavior of Zircaloy-4, DXB, and DXD4 cladding was measured at the maximum hoop strain location (location of cladding breach) for each stress rupture test specimen. Measurement results are given in Tables B.2 (Zircaloy-4), B.3 (DXB), and B.4 (DXD4).

The hoop strain data (hoop strain at the rupture location as a function of test temperature) for several lots of standard Zircaloy-4 cladding (with a nominal tin level of 1.5%) are shown in Figure D.8. The upper-bound curve for all of the data is indicated in the figure; this represents the maximum hoop strain reference curve for Zircaloy-4 cladding. Figure D.9 shows a comparison of the Zircaloy-4 cladding reference curve and the rupture hoop strain data for low-tin Zircaloy-4 cladding. In Figure D.10, the rupture hoop strains of DXD4 and DXB cladding are compared to the Zircaloy-4 cladding reference curve.

The maximum hoop strain of DXD4 cladding at temperatures between 700 and 900°C – the temperature range of greatest interest because superplastic deformation may take place at these temperatures – never exceeds the hoop strain of the reference Zircaloy-4 cladding. Fuel clad swelling in a LOCA transient is, therefore, no more severe for DXD4 cladding than for Zircaloy-4 cladding. Thus, analyses which indicate that fuel with Zircaloy-4 cladding would not suffer from coolant flow blockage during a transient are also applicable to fuel with DXD4 cladding, and would likewise indicate that flow blockage does not occur when DXD4 cladding is used.

**Table D.1 Zircaloy-4 Cladding Source and Properties**



**Table D.2 Stress Rupture and Clad Swelling Test Results for  
Zircaloy-4 Cladding with a Nominal Tin Content of 1.3%**



**Table D.2 Stress Rupture and Clad Swelling Test Results for  
Zircaloy-4 Cladding with a Nominal Tin Content of 1.3%**  
*(continued)*



**Table D.2 Stress Rupture and Clad Swelling Test Results for  
Zircaloy-4 Cladding with a Nominal Tin Content of 1.3%**  
*(continued)*



**Table D.3 Stress Rupture and Clad Swelling Test Results  
for Duplex D4 (DXD4) Cladding**



**Table D.4 Stress Rupture and Clad Swelling Test Results  
for Duplex B (DXB) Cladding**



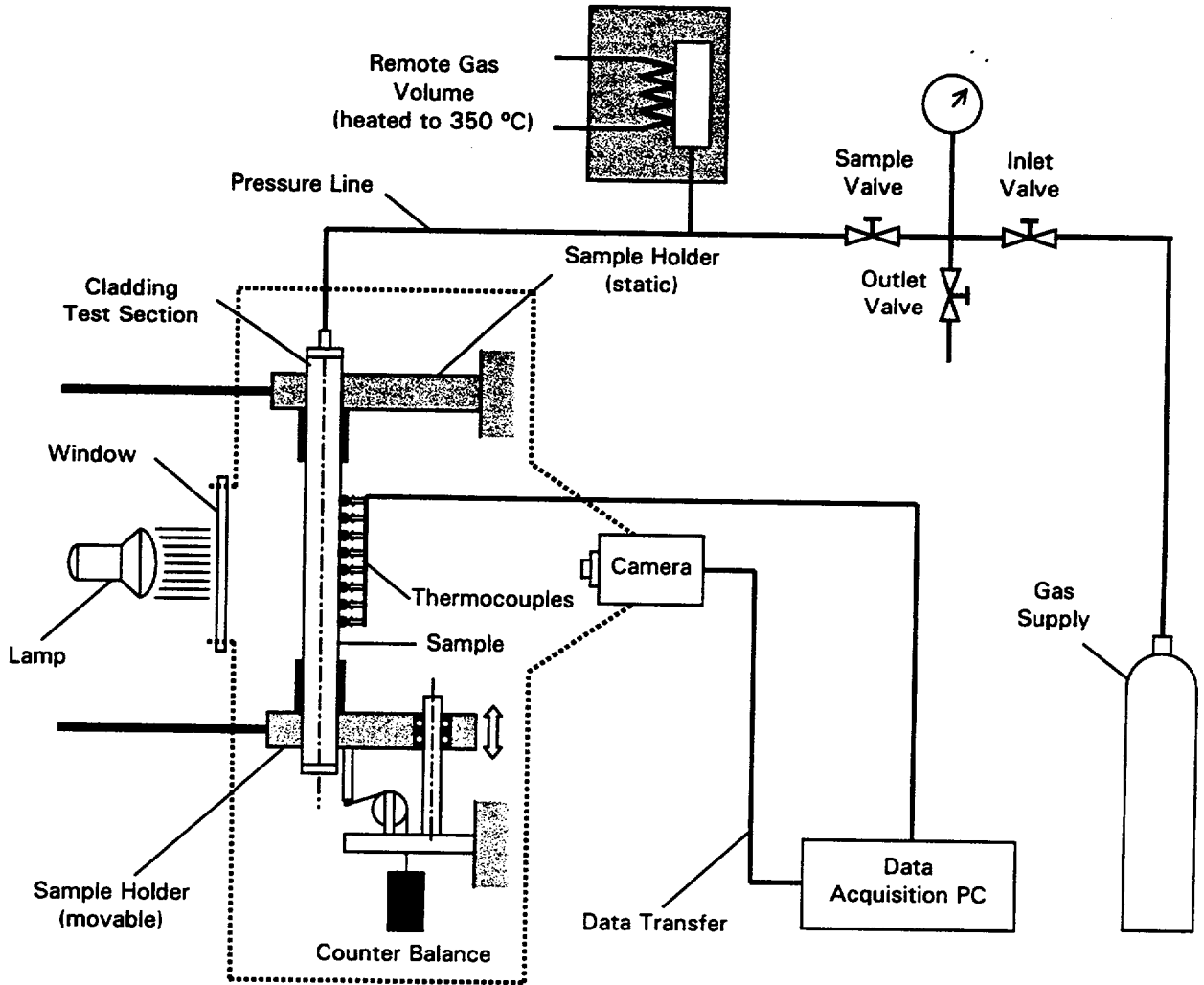


Figure D.1 Schematic Representation of Stress Rupture and Ballooning Test Experimental Setup

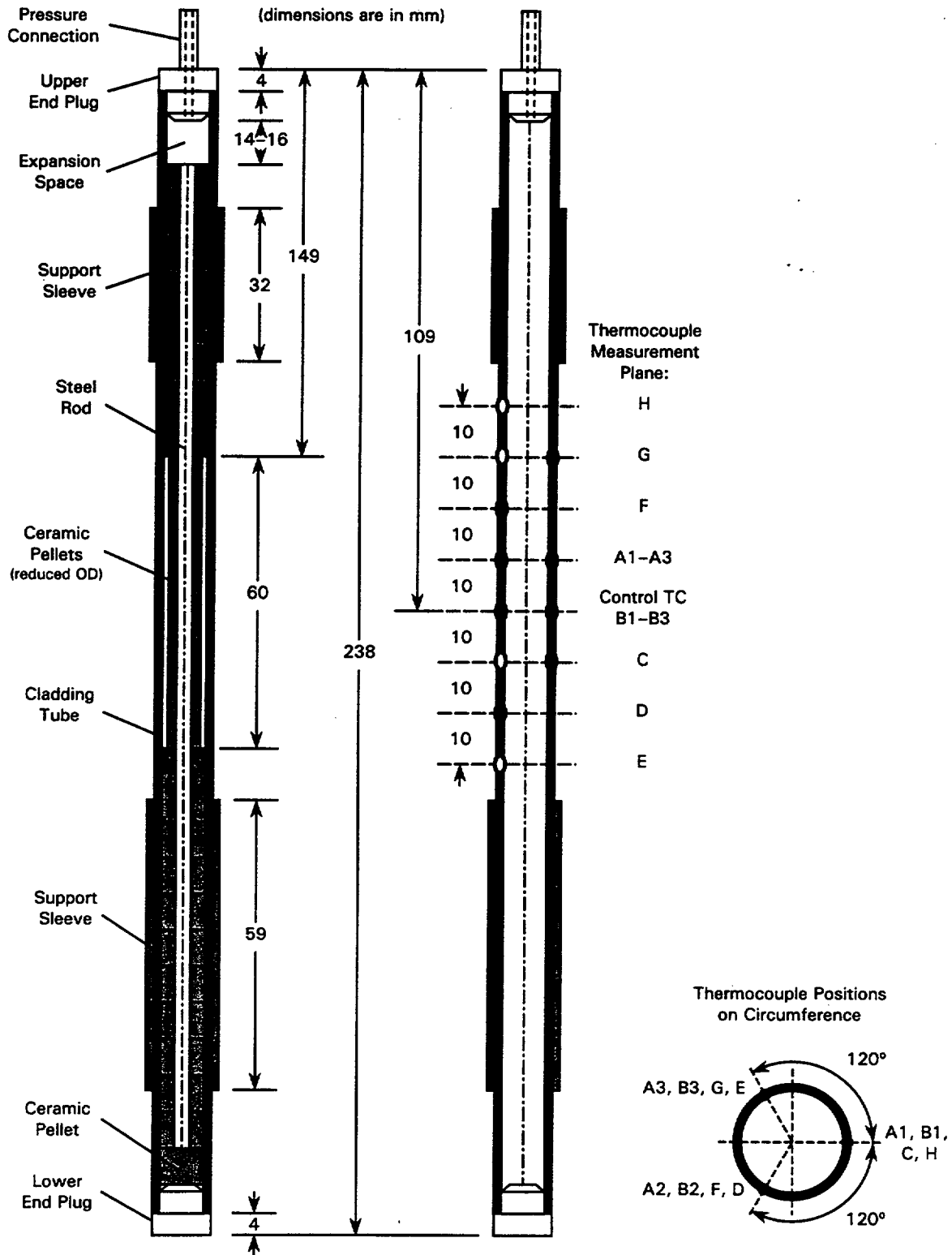


Figure D.2 Stress Rupture and Ballooning Specimen Design (left) and Thermocouple Locations (center and right)



**Figure D.3** Change of Temperature and Pressure as a Function of Time in the Stress Rupture Test



**Figure D.4** Typical Evolution of Strain During a Stress Rupture Test



**Figure D.5** Time to Rupture of Low-Tin Zircaloy-4 Cladding as a Function of Temperature and Initial Specimen Pressure



**Figure D.6** Time to Rupture of Standard-Tin (1.5% Sn) and Low-Tin (1.3% Sn) Zircaloy-4 Cladding as a Function of Temperature and Initial Cladding Hoop Stress  
*(These data are used to establish the least-squares fit reference lines for Zircaloy-4 cladding)*



**Figure D.7** Time to Rupture of DXD4 and DXB Cladding as a Function of Temperature and Initial Cladding Hoop Stress. *(The lines represent the Zircaloy-4 cladding reference correlations established earlier.)*



**Figure D.8** Hoop Strain at Rupture of Zircaloy-4 Cladding with a Nominal Tin Content of 1.5%. *(The upper-bound curve is the Zircaloy-4 cladding reference maximum hoop strain.)*



**Figure D.9** Hoop Strain at Rupture of Low-Tin Zircaloy-4 Cladding Compared to the Standard Zircaloy-4 Cladding Reference Maximum Hoop Strain



**Figure D.10** Rupture Hoop Strain of DXD4 and DXB Cladding Compared to the Standard Zircaloy-4 Cladding Reference Maximum Hoop Strain

Duplex D4 (DXD4) Cladding for PWRs

---

(This page was intentionally left blank.)

## Appendix E High-Temperature Corrosion and Quench Behavior

### Summary

High-temperature corrosion and quench tests were performed on specimens of Duplex D4 (DXD4) and standard through-wall Zircaloy-4 claddings to compare the behavior of the two types of cladding and to determine relevant properties for input into the loss-of-coolant accident (LOCA) analysis of fuel rods fabricated with DXD4 cladding. The quench test is used to confirm applicability of the 2200°F and 17% equivalent cladding reacted (ECR) criteria of 10 CFR 50.46 to DXD4 Cladding. Metallographic analysis was performed to confirm the integrity of the cladding after quenching and to determine the thickness of the oxygen-stabilized alpha layer on the inside and outside of the cladding.

Test results showed comparable weight gains and oxygen penetration for Zircaloy-4 and DXD4 cladding during high-temperature oxidation. Quench behavior was also the same for both materials. These results confirm that the metal-water reaction correlations established for fuel rods with Zircaloy-4 cladding can also be used for DXD4 clad rods.

### E.1. *Introduction*

High-temperature steam oxidation kinetics of zirconium-based alloys are required to determine the behavior of fuel rod cladding during a postulated LOCA in light water reactors. Isothermal oxidation and oxygen diffusion data are used in models to predict the oxidation behavior and the change in microstructure of the cladding during a temperature transient.

The experimental technique used by Siemens provides a comparison of the high-temperature steam oxidation of different zirconium-based alloys used as cladding materials. Although, because of specimen end effects (see Section E.4), the test overestimates the absolute values of the high-temperature corrosion kinetics, the test conditions realistically simulate the in-reactor conditions and are highly accurate for comparison with Zircaloy-4.

The evaluation of the test results of DXD4 cladding and the comparison with Zircaloy-4 also include data for other zirconium-based alloy and Duplex claddings (Zr 1.0 Nb, DXB, and Zr 2.5 Nb) that have previously been measured.

## **E.2. *Experimental Design***

The experimental setup, shown in Figure E.1, consists of a water-filled quartz container which holds the sample in the center of an induction coil in the lower extension tube. The upper part of the quartz container has a wider diameter, where heat, supplied in the lower part by the induction coil, is extracted by a cooling coil to prevent the water from evaporating. With this setup, very high heating and cooling rates can be used, providing realistic LOCA boundary conditions. For example, the boundary conditions of a steam blanket surrounding the specimen are realistic compared to fuel rod conditions in a LOCA.

The specimen is heated rapidly to the desired temperature with a 15 kW induction coil, causing the formation of a steam blanket at both the inner and outer surfaces of the specimen. The specimen is held at temperature by a fast electronic controller with feedback to the power supply of the induction heating unit. Specimen temperature is measured and monitored by a dual-wavelength pyrometer. The temperature signal of the pyrometer is fed back to an electronic controller and to a data acquisition unit in which the temperature signal is converted and stored. The pyrometer determines temperatures by computing the ratio of radiant energies emitted from the specimen surface in two separate, but nearly equal, wavebands. These signals are then processed by a single detector, which receives input from the target and from a constant-temperature reference source. The system operates as a null-seeking device by balancing the inputs from the reference and target sources. Accuracy and repeatability of the setup are determined by the reference source, which operates as a highly reproducible standard. The pyrometer, therefore, permits precise, drift-free operation during which specimen temperature is unaffected by low or changing target emissivities.

The temperature output of the pyrometer is calibrated using a special thick-wall sample with a fine Pt-PtRh thermocouple positioned axially in the center of the specimen length. Any difference in the temperature between the pyrometer and the thermocouple readings is

adjusted by the surface index factor control of the pyrometer. Such a difference can occur because the pyrometer measures through boiling water and the quartz wall of the container.

After the desired time at temperature, the system is de-energized and the specimen is quenched rapidly down to room temperature by the intensive cooling of the surrounding water bath. Figure E.2 shows a typical temperature-time history of a high-temperature corrosion-quench test. Temperature fluctuations during the test are caused by the highly turbulent water surrounding the specimen. Larger temperature fluctuations at the beginning of a test are due to the behavior of the induction coil.

At the conclusion of a test, the specimen is visually inspected, measured for weight gain and examined metallographically to determine the thickness of the oxide layer, the thickness of the oxygen-stabilized alpha-zirconium layer, and to evaluate microstructure. Metallographic transverse cross-sections are prepared through the middle of the specimen at the position of the temperature measurement by the pyrometer. The ECR value is determined from the weight gain of the specimen with the assumption that stoichiometric  $ZrO_2$  was formed.

### E.3. *Test Program*

The cladding used for the high-temperature corrosion and quench tests was standard production Zircaloy-4 and DXD4 cladding. Source and chemical composition information for the cladding used in the tests is given in Table E.1. Cladding tube specimens of 20 mm length, cut from the standard finished tubing, were cleaned and weighed prior to the tests. The weight gains and the behavior of the Duplex cladding were directly compared to those of Zircaloy-4 cladding.

The high-temperature corrosion tests were targeted for ECR values between approximately 5 and 20% at test temperatures of 1050, 1150, and 1250°C. Times at temperature varied from 60 to 600 seconds. ECR was calculated from the weight gain, assuming the formation of a uniform-thickness and stoichiometric  $ZrO_2$  layer over the total specimen surface. As explained in Section E.4, this leads to a slight overestimate of the corrosion

kinetics. Metallographic cross-sections were used to determine the thickness of the oxide layer and oxygen-stabilized alpha-zirconium layer.

#### E.4. *Test Results*

Uniformity of the temperature profile over the specimen length was not evaluated for these tests. Visual examinations of the specimens indicated that the ends of the tube sections had a somewhat higher oxide thickness and were, therefore, at a higher temperature than the center portions of the specimens. ECR values calculated from specimen weight were based on an assumed uniform-thickness corrosion layer and, therefore, were overestimated relative to the temperature recorded in the center of the specimen (which was lower than the specimen average temperature). For this reason, the tests were not used to determine the absolute values of the corrosion kinetics. However, the test conditions were realistic and were suitable for comparing the behavior of DXD4 and Zircaloy-4 cladding. Furthermore, for Duplex cladding, the corrosion kinetics for the D4 alloy of the outer layer can be directly compared to the kinetics of the Zircaloy-4 inner layer by inspection of the metallographic cross-sections.

##### E.4.1 Corrosion Kinetics

Assuming corrosion kinetics to be a parabolic function of time, the weight gain of the cladding specimens, given in Tables E.2 (Zircaloy-4 cladding) and E.3 (DXD4 cladding), was plotted as a function of the square root of exposure time in Figures E.3 and E.4 for Zircaloy-4 and DXD4 cladding, respectively. Figure E.5 compares the weight gain results for the two types of cladding. The linear correlations shown in the figures confirm the parabolic kinetics and allow the determination of a kinetics constant for each temperature. Determination of the kinetics constants from the weight gain, however, would lead to an overestimate of the corrosion rate because of specimen end effects and oxygen uptake in the cladding (oxygen-stabilized alpha layer). The test results for DXD4 and Zircaloy-4 cladding specimens tested under the same conditions are, therefore, simply compared to one another to determine if correlations for Zircaloy-4 can be applied to DXD4 cladding.

Metallographic cross-sections of cladding specimens are shown in Figures E.8 through E.19. As shown in the metallographs, none of the cladding specimens (up to 25% ECR)

showed through-wall cracks. In specimens with thicker oxide scale, cracks are formed upon quenching. The cracks may extend through the oxide scale and oxygen-stabilized alpha layer, but all cracks are arrested at the as-beta-quenched innermost layer.

In general, the oxide scale on a cladding specimen was thicker near the ends of the specimen than in the center, at the location where the temperature was measured and controlled during the test. For this reason, the corrosion rate calculated from the average weight gain is slightly overestimated. However, for a given test temperature and specimen size, test results for different cladding types may be readily compared. Such a comparison (see Figure E.5) shows that the corrosion rate of DXD4 cladding at high temperatures is slightly lower than that of Zircaloy-4 cladding.

#### E.4.2 Metallography

Several of the cladding specimens were metallographically examined after the high-temperature oxidation and quenching tests. Samples were cut parallel and perpendicular to the tube axis near the center of selected specimens. The integrity of the samples was checked and the thicknesses of the corrosion layer, the oxygen-stabilized alpha layer, and the beta-quenched center part of the cladding wall were measured; data are given in Tables E.2 and E.3. Representative micrographs are shown in Figures E.8 through E.19.

Both the inside (Zircaloy-4) and outside (D4 alloy) surfaces of the cladding specimen were covered with a uniform oxide scale formed during the corrosion at high temperature. Underneath the oxide scale, on both sides of the cladding, an oxygen-stabilized alpha layer had formed. The thickness of these layers, both inside and outside, was measured and recorded, and is reported in Tables E.2 and E.3.

The thickness of the oxide scale on the D4 alloy which makes up the DXD4 cladding's outer surface was, in general, the same as the thickness of the scale on the cladding's Zircaloy-4 inner surface, as shown in Figure E.6, where the measured oxide thicknesses of the D4 and Zircaloy-4 layers are plotted as a function of ECR. The thickness of the oxygen-stabilized alpha layer on the cladding's D4-alloy outer surface was, in most cases, slightly less than that of the Zircaloy-4 inner surface, as shown in Figure E.7. Differences are considered minor, however, and the metallographic observations confirm that there are

no significant differences in high-temperature corrosion behavior of Zircaloy-4 and the D4 alloy, or between Zircaloy-4 cladding and DXD4 cladding.

Many of the micrographs presented in Figures E.8 through E.19 show cracks that occurred upon quenching from high temperature. These cracks most frequently appear in the micrographs as white lines in the oxygen-stabilized alpha layer. Visual inspection of the metallographic samples confirms the integrity of the rapidly quenched cladding specimens. The cracks, more pronounced in the longer-term-exposure samples, penetrate through the oxide scale and into the oxygen-stabilized alpha layer, but never penetrate into the beta-quenched center part of the cladding wall. This observation is in agreement with earlier findings by Chung et. al. (Reference E.1), wherein it was observed that cladding failures occur only when all of the remaining metal part of the cladding consists of oxygen-stabilized alpha phase and no as-beta-quenched material remains.

DXD4 cladding specimens were carefully inspected for de-bonding of the interface between the D4 and Zircaloy-4 layers. After the corrosion-quench tests, the transition from D4 to Zircaloy-4 could not be readily discerned because the small difference in the chemical composition of the two layers does not lead to easily observable differences in microstructures. De-lamination of the layers was never observed, and none of the micrographs showed any cracks parallel to the cladding wall surfaces.

#### E.5. *Conclusions*

The results of the high-temperature corrosion and quench tests may be summarized as follows:

- DXD4 cladding and Zircaloy-4 cladding show comparable high-temperature (1050 to 1250°C) corrosion behavior when exposed in a steam-saturated environment.
- High-temperature corrosion of DXD4 cladding is conservatively described by correlations developed for Zircaloy-4.
- The 2200°F and 17% ECR criteria can be applied to DXD4 cladding and other Zircaloy-4-based Duplex claddings because tests up to 25% ECR do not lead to cladding failure upon rapid quenching in water from high temperature.
- De-bonding of the D4 alloy outer layer and the Zircaloy-4 inner layer substrate is not observed during either high-temperature corrosion or upon quenching from high temperature.

**E.6. References**

- E.1 H. M. Chung et al., "Development of an Oxygen Embrittlement Criterion for Zircaloy Cladding Applicable to Loss-of-Coolant Accident Conditions in Light-Water Reactors," *Zirconium in the Nuclear Industry (fourth Conference)*, ASTM STP 681, American Society for Testing and Materials, 1979, pp. 600-627.

**Table E.1 Cladding Source and Chemical Composition Records for  
High-Temperature Corrosion and Quench Test Specimens**



**Table E.2 Results of High-Temperature Corrosion Tests  
on Through-Wall Zircaloy-4 Cladding**



**Table E.3** Results of High-Temperature Corrosion Tests  
on Duplex D4 Cladding



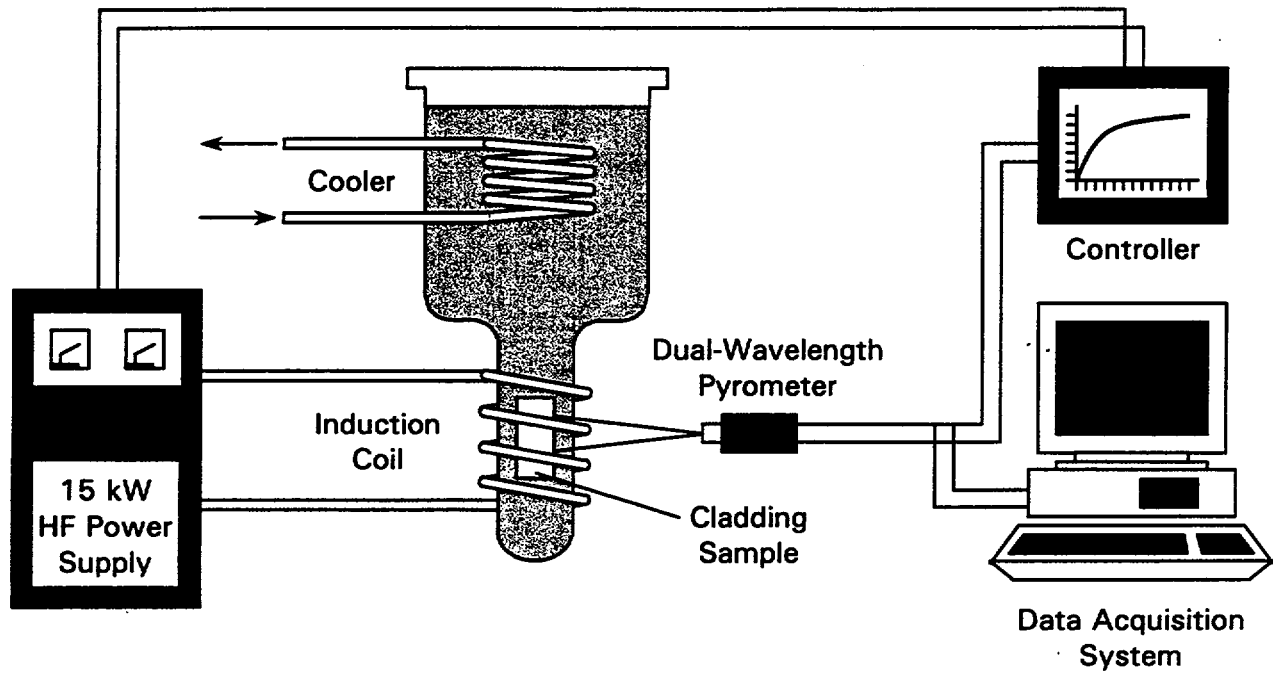


Figure E.1 Apparatus for the Determination of High-Temperature Steam Oxidation Kinetics of Zirconium Alloy Cladding

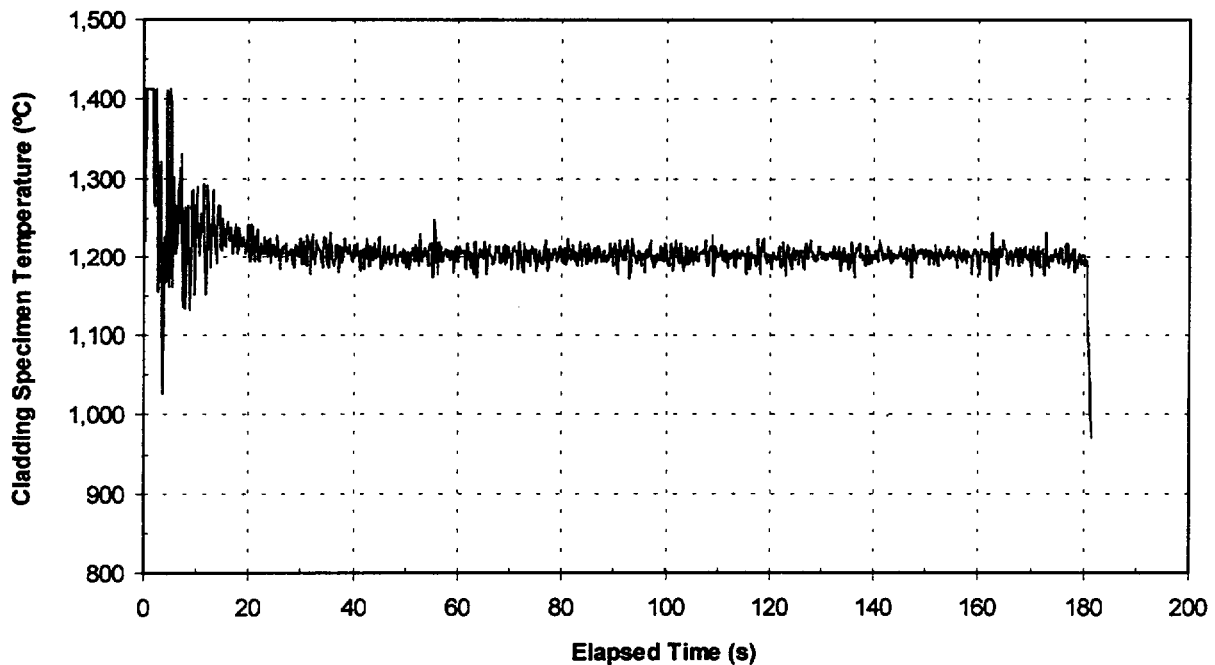


Figure E.2 Typical Example of Cladding Specimen Temperature as a Function of Time During a High-Temperature Oxidation and Quench Test



**Figure E.3** Weight Gain as a Function of Time for Through-Wall Zircaloy-4 Cladding



**Figure E.4** Weight Gain as a Function of Time for Duplex D4 Cladding



**Figure E.5** Comparison of Weight Gain as a Function of Time  
for Through-Wall Zircaloy-4 and Duplex D4 Cladding



**Figure E.6** Thickness of the Oxide Scale on the Zircaloy-4 Inner Surface  
and D4-Alloy Outer Surface of Duplex D4 Cladding Specimens.  
*(The thickness of the oxide scale on both surfaces is identical.)*



**Figure E.7** Thickness of the Oxygen-Stabilized  $\alpha$ -Layer of the Zircaloy-4 Inner Surface and D4-Alloy Outer Surface of Duplex D4 Cladding Specimens.  
*(Oxygen penetration is, in general, somewhat greater in Zircaloy-4 than in the D4 Alloy.)*



**Figure E.8 Duplex D4 Cladding Exposed for Ten (10) Minutes at 1050°C**



**Figure E.9** Duplex D4 Cladding Exposed for Five (5) Minutes at 1050°C



**Figure E.10** Duplex D4 Cladding Exposed for Two (2) Minutes at 1050°C



**Figure E.11 Duplex D4 Cladding Exposed for One (1) Minute at 1050°C**



**Figure E.12** Duplex D4 Cladding Exposed for Ten (10) Minutes at 1150°C



**Figure E.13** Duplex D4 Cladding Exposed for Two (2) Minutes at 1150°C



**Figure E.14** Duplex D4 Cladding Exposed for One (1) Minute at 1150°C



**Figure E.15** Duplex D4 Cladding Exposed for Ten (10) Minutes at 1250°C



**Figure E.16** Duplex D4 Cladding Exposed for Two (2) Minutes at 1250°C



**Figure E.17** Duplex D4 Cladding Exposed for One (1) Minute at 1250°C

## Distribution

### Controlled Distribution

#### Richland

F. T. Adams, 21  
V. I. Arimescu, 31  
M. R. Billaux, 31  
C. A. Brown, 31  
J. M. Burnett, BV  
D. J. Denver, 38  
W. C. Dey, 33  
R. L. Feuerbacher, 21  
J. A. Ford, 31  
J. S. Holm, 26  
T. M. Howe, 31  
M. A. Jaeger, 33  
J. F. Mallay, 26  
R. E. Narum, 31  
R. A. Perkins, 31  
R. S. Reynolds, 21  
S.-H. Shann, 31  
L. G. Stephens, 42  
L. F. Van Swam, 31

#### Erlangen

H. Lettau  
R. Manzel  
A. Seibold  
H.-J. Sell